

Chirality in bare and ligand-protected metal nanoclusters

J. Jesús Pelayo, Israel Valencia, A. Patricio García, Le Chang, Marta López, Daniele Toffoli, Mauro Stener, Alessandro Fortunelli & Ignacio L. Garzón

To cite this article: J. Jesús Pelayo, Israel Valencia, A. Patricio García, Le Chang, Marta López, Daniele Toffoli, Mauro Stener, Alessandro Fortunelli & Ignacio L. Garzón (2018) Chirality in bare and ligand-protected metal nanoclusters, *Advances in Physics: X*, 3:1, 1509727, DOI: [10.1080/23746149.2018.1509727](https://doi.org/10.1080/23746149.2018.1509727)

To link to this article: <https://doi.org/10.1080/23746149.2018.1509727>



© 2018 The Author(s). Published by Informa UK Limited, trading as Taylor & Francis Group.



Published online: 15 Sep 2018.



[Submit your article to this journal](#)



Article views: 1326



[View related articles](#)



[View Crossmark data](#)



Citing articles: 4 [View citing articles](#)

Chirality in bare and ligand-protected metal nanoclusters

J. Jesús Pelayo^a, Israel Valencia^b, A. Patricio García^c, Le Chang^{d,e}, Marta López^f, Daniele Toffoli^f, Mauro Stener^f, Alessandro Fortunelli^d and Ignacio L. Garzón^c

^aEscuela Superior de Apan, Universidad Autónoma del Estado de Hidalgo, Chimalpa Tlayote, Apan, Mexico; ^bLaboratorio de Fitoquímica, Unidad de Biotecnología y Prototipos, Facultad de Estudios Superiores-Iztacala, Universidad Nacional Autónoma de México, Tlanepantla, Estado de México, Mexico; ^cInstituto de Física, Universidad Nacional Autónoma de México, CDMX, Mexico; ^dCNR-ICCOM, Consiglio Nazionale delle Ricerche, Pisa, Italy; ^eBeijing Key Laboratory of Energy Environmental Catalysis, Beijing University of Chemical Technology, Beijing, People's Republic of China; ^fDipartimento di Scienze Chimiche e Farmaceutiche, Università di Trieste, Trieste, Italy

ABSTRACT

Chirality is a fundamental property of matter with profound impact in physics, chemistry, biology, and medicine. It is present at several scales going from elementary particles, to molecules, to macroscopic materials, and even to astronomical objects. During the last 30 years, chirality has also been investigated at the nanoscale, being a hot research topic in nanoscience. The importance of chirality at the nanoscale is due, in part, to the potential applications that chiral nanomaterials could have in nanotechnology. Great interest exists nowadays in the study of chirality in bare and ligand-protected metal nanoclusters. These are aggregates of n metal atoms ($n \sim 10\text{--}300$) that can be in gas phase or stabilized by organic ligands, covering the cluster surface. Chirality in bare and thiolate-protected gold clusters (TPGC) has received special attention because of the important progress achieved in their synthesis, size separation, and precise structural characterization. Here, we review the recent experimental and theoretical developments on the origin and physicochemical manifestations of chirality in bare and TPGC. Since chirality is a geometrical property, we also discuss the proposal for its quantification, and the correlation of this geometric measure with the chiroptical response, like the circular dichroism spectrum, calculated from quantum mechanical methods.

ARTICLE HISTORY

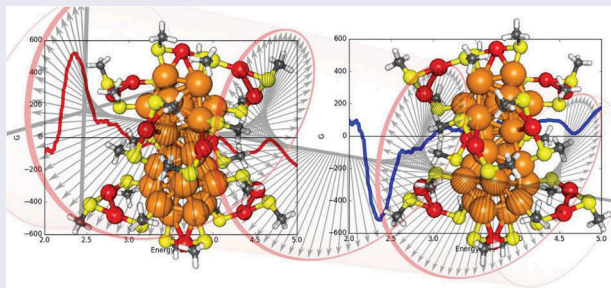
Received 12 February 2018
Accepted 1 August 2018

KEYWORDS

Chirality; metal clusters; gold clusters; circular dichroism; Hausdorff chirality measure; time-dependent density functional theory

PACS

36.40.-c Atomic and molecular clusters; 36.40.Mr Spectroscopy and geometrical structure of clusters; 61.46.Bc Structure of clusters; 78.67.Bf Optical properties of nanocrystalsnanoparticles nanoclusters



CONTACT Ignacio L. Garzón  garzon@fisica.unam.mx  Instituto de Física, Universidad Nacional Autónoma de México, Apartado Postal 20-364, CDMX 01000, Mexico

© 2018 The Author(s). Published by Informa UK Limited, trading as Taylor & Francis Group.

This is an Open Access article distributed under the terms of the Creative Commons Attribution License (<http://creativecommons.org/licenses/by/4.0/>), which permits unrestricted use, distribution, and reproduction in any medium, provided the original work is properly cited.

1. Introduction

1.1. Chirality

Chirality has been of great interest for science and industry since the discovery of chiral substances in the nineteenth century [1,2]. This phenomenon quickly captured the attention of scientists, particularly Louis Pasteur, who first separated optical isomers and speculated that chirality was originated on the atomic arrangements of atoms [3]. By the end of the nineteenth century, it was Lord Kelvin who coined the term chirality, which was previously called 'dissymmetry' [4]. Chirality is a geometrical property where an object cannot be superimposed with its mirror image. So, to be chiral the object should not have any S_n symmetry elements such as mirror planes or inversion symmetry. This property is intrinsic to an object and it is not restricted to the molecular level, as chirality can be observed in any scale, for example, in single molecules, DNA, viruses, our hands, or even in galaxies (see Figure 1) [5–7].

One of the most important properties of chiral particles is their unique optical activity, which is measured by the circular dichroism (CD) spectrum. When chiral particles are in solution and circularly polarized light passes through them, it causes a difference in the absorption between the right and left polarized light. The difference in absorption is measured resulting in the CD spectrum of the chiral particle [8]. CD is useful to analyse the structures of chiral molecules. Light can interact in several ways with chiral particles, for instance, electronic absorption, vibrational absorption, reflection, scattering, or fluorescence [9]. Different methods have been developed based on these interactions, such as electronic CD [10], vibrational CD [11], diffuse reflection CD [12], circularly polarized luminescence [13], magnetic CD [14], and optical rotatory dispersion [15].

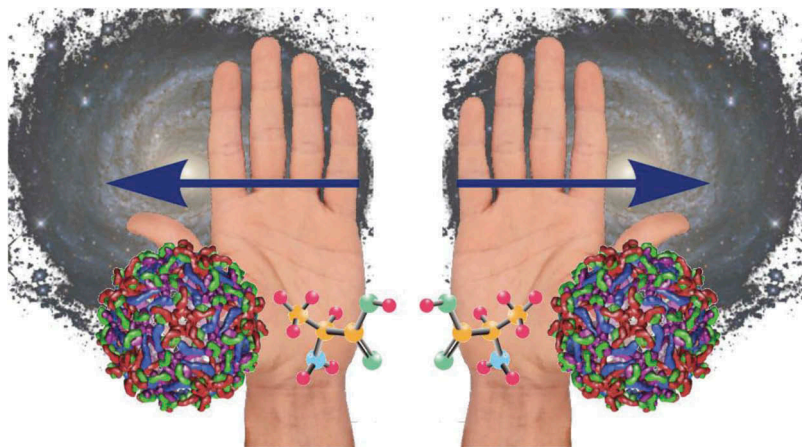


Figure 1. Different chiral systems that exist in our universe.

1.2. Importance of chirality

When chiral substances and its properties were discovered, they became a major topic in chemistry and biology, as they play an important role in the life of plants and animals. Methods for enantioselective synthesis, catalysis, and new pharmaceuticals were promptly developed [16–18]. Nowadays, chirality is important in many areas of science. In biology, the chirality of biomolecules is of great relevance [2], the DNA chiral structure as well [19]. Additionally, chirality is believed to be one of the keys to the origin of life and evolution [20]. In medicine, chirality plays a relevant role in methods for the detection of diseases [21], as well as in drug design because it allows for the identification and separation of enantiomers of the active substance, something of crucial importance because the biological activity (pharmacology, toxicology, and metabolism) can greatly vary depending on the drug enantiomer used [22,23]. Chemistry itself has benefited greatly from chirality because it has allowed many advances in the areas of enantioselective synthesis [24], separation [25], catalysis [26] and chiral sensing [27].

1.3. Chirality at the nanoscale

At some point, it was believed that chirality was an exclusive property of organic molecules, but Alfred Werner proved, with the synthesis of coordination complexes, that inorganic substances were chiral too [28]. Inorganic materials have come a long way since then and chirality in nanoscience has become a ‘hot topic’, in fact, the research and development of nanomaterials has increased exponentially [29–31]. The theory of chirality for molecules is already well established, but for metals, semiconductors, and nanostructures, the concept of chirality is still evolving. With all this expansion, there has been a lot of interest in the properties of chiral nanomaterials [32,33]. Chiral nanomaterials have an impressive range of applications in biomedicine [34], catalysis [35], and optical devices [36], but they also offer the opportunity to gain insights into the origin of chirality, as they serve as a middle ground between chiral molecules and chiral macroscopic objects. Another advantage of chiral nanomaterials is that their properties can be finely tuned for their study, according to their size, shape, and composition [37–39]. In general, a nanoparticle (NP) is any particle which size is between 0.5 and 100 nm and its shape might be chiral. Some of the nanostructures in which chirality has been found are nanoribbons [40], nanowires [41–44], metal nanoclusters [45], nanoalloys [46–48], semiconductor NPs [49], metal oxide NPs [50], carbon NPs [51], and others [52–55]. Generally, the shapes of the nanostructures are not perfectly symmetrical, because they often present dislocations, vacancies,

atoms, truncations, and deformation, thus contributing to the chirality of the nanostructures. CD has been observed in these nanostructures, and the source of the electronic excitation can be caused because of (i) chiral shapes, (ii) chiral assembly of interacting achiral NPs, and (iii) interaction of NPs with molecules (see [Figure 2](#)) [9,29,56].

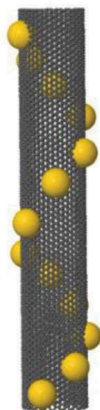
The first type of nanostructure with a chiral shape is found in twisted nanorods [57], twisted gold clusters [58], twisted ribbons [59], and helical structures of gold [60], silica [61], and TiO_2 [62]. In these structures, the CD can be observed in the plasmonic region, and the temperature independence of the plasmonic CD can be used to confirm the presence of the chiral NPs [63,64]. The second type of chirality arises from a chiral configuration of various achiral NPs. This is especially effective with plasmonic NPs because it leads to plasmon coupling of the NPs [65]. The optical activity of the assemblies is dependent on the total size, and their preparation typically requires advanced chemistry or the use of chiral biomolecules as templates to control their positions and interactions [66–68]. The third type of chirality can be caused because of two effects: the first is the transfer of chirality from chiral molecules to an achiral metal core as observed by Whetten et al., in 1998 [69], and the second one is the formation of chiral patterns by achiral ligands [70].

Metal clusters are a special type of nanomaterials because of their atomic precision, as their size corresponds to a discrete number of atoms, the ‘magic numbers’ [71]. Their size can vary from few to thousands of atoms. Moreover, metal clusters can be protected with a monolayer of ligands, e.g.

i) Chiral shapes



ii) Chiral assemblies



iii) Chirality induced by ligands

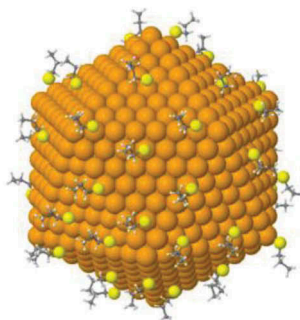


Figure 2. Three causes of chirality in nanostructures. (i) The helical structure of a gold tetrahedral nanowire. (ii) Gold NPs adsorbed on a carbon nanotube in a chiral assembly. (iii) Chirality induced on a symmetrical cluster by the asymmetrical arrangement of the ligands on its surface.

thiolates, phosphines, selenolates, and others [72–75]. The ligands bring stability to the metal core by helping avoid aggregation and regulating the number of valence electrons in the nanocluster [76]. Chirality has also been found, and geometrically quantified, in bare and ligand-protected metal clusters [77]. In this review, we briefly present the research highlights on the chirality shown by bare and thiolate-protected gold clusters (TPGC) published during the last 20 years (Section 2), followed by a revision of the proposal and convenience of quantifying the chirality existent in bare and TPGC from a geometrical point of view (Section 3). In Section 4, we provide an overview of the quantum mechanical methods that can calculate in a reliable way the CD spectrum of TPGC clusters with few hundreds of atoms. Section 5 is dedicated to present recent evidence on the correlation existing between the geometrical measure of chirality and the chiroptical response (calculated CD spectra). A summary and perspectives on the investigation of chirality in metal nanoclusters is presented in Section 6.

2. Chirality in bare and thiolate-protected gold clusters

2.1. Thiolate-protected gold clusters

Chirality in TPGC was first detected in 1998–2000, following the measurements of intense optical activity in L-glutathione-protected gold clusters in the size range of ~20–40 Au atoms (L-glutathione is a chiral tripeptide ligand) [69,78]. During the last 20 years, a lot of progress has been made on the controlled synthesis, size and enantiomeric separation, total structural characterization, and chiroptical spectroscopic studies of chiral TPGC, as well on the theoretical origin and understanding of their chirality. Several research reviews have been published highlighting these advances and providing updated results on unsolved questions surged during this 20-year period [9,58,75,79–87].

For example, by the year 2007, after the experimental confirmation by several research groups on the existence of optical activity in gold clusters protected by chiral ligands, three mechanisms were proposed towards the understanding of the origin of their chirality: the intrinsically chiral metal cluster core [88], the dissymmetric field effect [89], and the chiral footprint model [90]. These mechanisms, supported by consistent theoretical models and calculations, provided useful qualitative explanations on the unique features displayed by the optical activity, measured for gold clusters with distinct sizes, and protected with different chiral ligands. Nevertheless, there was not a consensus on which of these mechanisms would play the dominant role, or if two, or all of them would act concurrently for a full understanding of the CD spectra and elucidate if the

chirality is either localized on the volume or surface of the metal core, or at the interface with the shell of chiral ligands [79–81]. Furthermore, by the year 2007, it was recognized that a precise knowledge of the atomic configuration existing in the optically active chiral compounds was necessary, as well as a reliable quantum mechanical methodology to calculate their electronic structure, including the ground and excited electronic states, to get real progress in the understanding of their chirality [79–81]. In fact, around that time there was a limited progress on the theoretical knowledge of the most stable (lowest energy) atomic structures of TPGC, and on the first-principle calculation of their CD spectra [88,91]. This was mainly due to the lack of sufficient computational resources and efficient implementations of the corresponding theoretical methodologies, given the substantial number of atoms and electrons involved.

A breakthrough in the field of TPGC occurred by the end of 2007 when the synthesis, crystallization, and total X-ray structure determination of the first chiral TPGC were reported. It corresponded to a *p*-mercaptobenzoic acid (*p*-MBA)-protected gold cluster, which comprises 102 gold atoms and 44 achiral *p*-MBAs ligands: Au₁₀₂(*p*-MBA)₄₄ [92]. This experimental study revealed not only the existence of a chiral cluster, since the two enantiomers were observed alternating in the crystal lattice, but also that protecting achiral ligands could be placed in a chiral array, forming ‘staple’ motifs on the surface of a nearly symmetric Marks decahedron Au₇₉ metal core [92]. Later, in 2010, this type of chiral structure was also found in a similar experimental study, as well as from a theoretical investigation, in a cluster with 38 gold atoms and 24 phenylethylthiolate (SC₂H₄Ph) achiral ligands [93,94]. In this case, the chiral Au₃₈(SC₂H₄Ph)₂₄ cluster was described as a 23-atom nearly symmetric core protected by a chiral arrangement of staple motifs [93,94]. The discovery of Au₁₀₂- and Au₃₈-protected gold clusters expanded the variety of chiral TPGC to include the case of a nearly symmetric (achiral) core protected with achiral ligands, where the chirality appears from the chiral patterns described by the staple motifs. **Figure 3** displays the structures of these chiral clusters.

Another breakthrough in the experimental study of chiral TPGC was the first enantiomeric separation of the chiral Au₃₈(SC₂H₄Ph)₂₄ cluster by high-performance liquid chromatography (HPCL), and the measurement of the corresponding mirror-image CD spectra with a huge anisotropy factor of up to 4×10^{-3} [95]. This work also allowed for a useful comparison with the calculated CD spectra, and for testing the reliability of more advanced quantum mechanical methodologies, that started to be developed by 2010 [94,95]. Thus, through a more accurate theoretical–experimental comparison between CD spectra, additional insights into the origin of the optical activity due to the electronic structure of chiral TPGC were obtained [94,96]. It is

worthwhile to mention that up to date, other chiral TPGC like $\text{Au}_{40}(\text{SC}_2\text{H}_4\text{Ph})_{24}$ [97] and $\text{Au}_{28}(\text{TBBT})_{20}$ (TBBT: p-tertbutylbenzenethiol) [98] have also been enantioseparated through HPLC, while a partial enantioenrichment has been achieved for the chiral $\text{Au}_{102}(\text{p-MBA})_{44}$ cluster [99]. Systematic chiroptical spectroscopic studies coupled with thermal-induced racemization have also determined that the gold-thiolate interface is quite flexible, a fact which is of fundamental interest to be considered in applications of chiral TPGC [100].

After the great progress achieved during the last 10 years, mainly based on the precise knowledge of the cluster structure by X-ray crystallography (XRC) of around 30 TPGC in the size range of 18–279 Au atoms, and on the detailed investigations using chiroptical spectroscopy on other TPGC dissolved in different solvents, there is a convincing evidence that many of them correspond to chiral clusters [9,58,75,77,80–87]. Moreover, the current view on chiral TPGC indicates that their chirality can be classified into intrinsic and induced one [84–86]. In the first case, the structure of the $\text{Au}_n(\text{SR})_m$ cluster can be divided into an inner metal core, an intermediate Au-S interface, and the external carbon tail of the organic ligands [84–86]. Then, the intrinsic chirality could be due to the chiral structure of the metal core or could be related with the chiral arrangement of the Au-S motifs, or also could be ascribed to the chiral arrangement of the carbon tails [84,85]. Figure 3 shows the structures of the chiral $\text{Au}_{44}(\text{SR})_{28}$ and $\text{Au}_{52}(\text{SR})_{32}$ clusters, where the metal core is formed by tetrahedral motifs following helicoidal (chiral) patterns. In this classification, it is considered that the thiolate ligands are achiral. On the other hand, chirality can be induced by chiral ligands protecting a metal core, like the chiral L-glutathione ligand used by Schaaaff and Whetten in 1998–2000, when they detected optical activity for the first time in TPGC [69,78].

2.2. Bare gold clusters

Chirality in bare metal (gold) clusters had also been investigated since 2002 when it was theoretically obtained that the lowest-energy isomers of Au_n clusters with $n = 28$ and 55 correspond to chiral structures [88,101]. Later, in 2007, three groups published convincing evidence, both experimental [102,103] and theoretical [104], on the existence of a chiral structure for the anionic cluster Au_{34}^- . Another theoretically predicted chiral cluster was Au_{72} , better known as a golden fullerene with chiral-icosahedral symmetry [105]. Figure 4 shows the structures of the chiral Au_{34}^- , Au_{55} , and Au_{72} gold clusters. More recently, a series of chiral gold nanocage structures have been theoretically predicted [106]. A research challenge for the future would be to accomplish the enantioseparation of these chiral bare gold clusters in order to explore at a more fundamental level their intrinsic chirality.

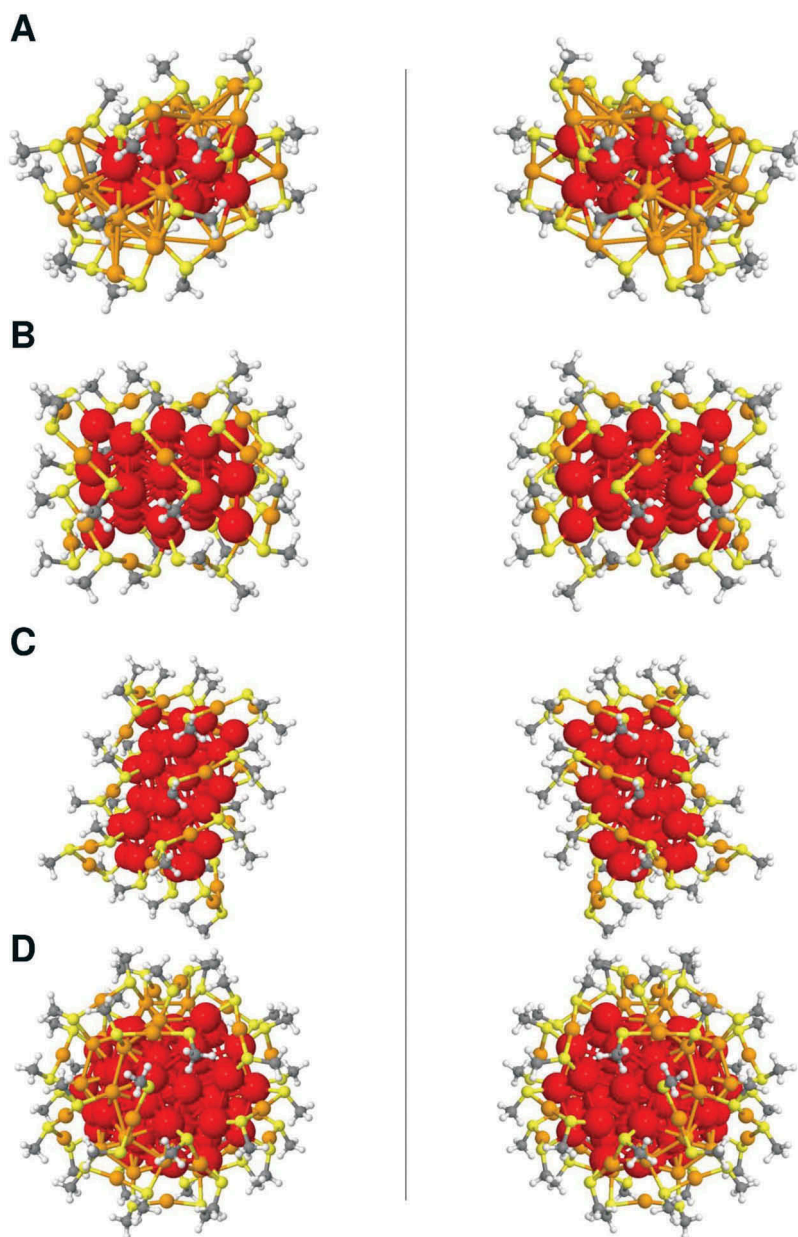


Figure 3. Structures of chiral thiolate-protected gold clusters. (a) $\text{Au}_{38}(\text{SCH}_3)_{24}$, (b) $\text{Au}_{44}(\text{SCH}_3)_{28}$, (c) $\text{Au}_{52}(\text{SCH}_3)_{32}$, and (d) $\text{Au}_{102}(\text{SCH}_3)_{44}$.

To gain additional and deeper insights into the origin of chirality, further studies have been performed, like the geometric quantification of chirality and the theoretical calculation and experimental measurement of the CD spectra. The following sections review the recent highlights of these investigations.

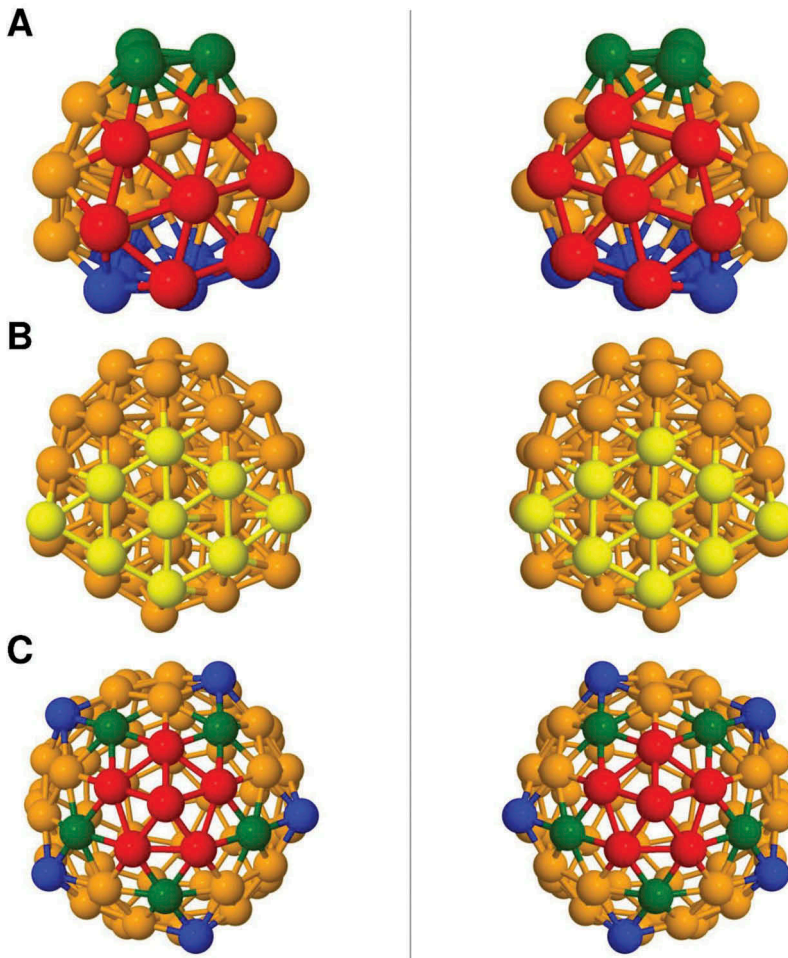


Figure 4. Structures of four bare chiral gold clusters. (a) Au_{34} , a chiral isomer with C_3 symmetry. (b) Au_{55} , a chiral isomer with C_1 symmetry. (c) Au_{72} , a chiral isomer with icosahedral (I) symmetry.

3. Geometric quantification of chirality

From the most fundamental point of view, chirality at any scale should be considered as a geometrical property, independent of its physical and chemical manifestations. This was first recognized by Lord Kelvin in his definition of chirality in 1893: I call any geometrical figure, or group of points ‘chiral’, and say that it has chirality if its image in a plane mirror, ideally realized cannot be brought to coincide with itself [4]. It is noteworthy that this definition of chirality has been mostly used in a dichotomic manner in chemistry, biology, and medicine. For example, a molecule is considered either chiral or achiral, if it does or does not satisfy the Kelvin’s definition. Nevertheless, one of the main objectives of physics is not only to discover, understand, and predict the properties of matter, but

also to quantify them. Then, from a physical point of view, it would be valid to ask the question if chirality can be continuously quantified, instead of only having 0 and 1 values for achiral and chiral systems, respectively. The proposal about the possibility and pertinence of quantifying the degree or amount of chirality was broadly discussed in 1992 in the context of molecular chirality, due to its importance in several fields of chemistry and biochemistry [107]. Since then, different related approaches had been proposed for a geometric quantification of molecular chirality [107–109]. Moreover, it has also been discussed that molecular chirality measures could be related to chemical manifestations like enantioselectivity in asymmetric catalysis [110].

An obvious and important question after recognizing the existence and relevance of chirality in bare and ligand-protected metal clusters (see Section 2) would be if it can be geometrically quantified and correlated with their physical and chemical properties. The initial answer to this question was given in 2002, when the Hausdorff chirality measure (HCM) [111] was used to quantify the chirality of bare Au_{28} and Au_{55} gold clusters, as well as of thiolate-protected $\text{Au}_{28}(\text{SCH}_3)_{16}$ and $\text{Au}_{38}(\text{SCH}_3)_{24}$ gold clusters [88,101] (see Appendix A for a detailed description of the definition and methodology to calculate the HCM). In that year, these clusters were of great interest since their structures were obtained from reliable *state of the art* density functional calculations [112,113], after the experimental discovery on the existence of optical activity in glutathione-protected gold clusters with sizes in the range of 20–40 gold atoms [69,78]. One of the initial insights into the origin of chirality obtained by geometrically quantifying it through the HCM was to show that chiral structures could exist as the lowest-energy isomers of bare gold clusters like Au_{55} and Au_{34}^- and that the thiolated protecting monolayer could induce or increase the degree of chirality of the metal cluster core [88,101]. Moreover, these results provided theoretical support for the existence of chirality in glutathione-protected gold clusters, as indicated by the strong optical activity measured in these compounds since 1998–2000 [69,78].

As was discussed in Section 2, the study of chirality in TPGC evolved in a dramatic fashion, especially after 2007, when the total X-ray structure of the $\text{Au}_{102}(\text{p-MBA})_{44}$ clusters determined its chiral morphology [92]. In fact, during the last 10 years, a huge amount of chiral thiolate-protected gold clusters have been synthesized, purified, and crystallized. Their total atomic structures have been fully determined from XRC, providing precise information to investigate further details on the origin of their chirality. Once such useful structural information was available, new questions related to the geometric quantification of chirality were raised [77]. Some of them question if it is possible to consistently compare the index of

chirality between different chiral clusters and classify them accordingly. Likewise, what is the ultimate origin of chirality given that the precise atomic structure of the chiral cluster is known? Or, is it possible to obtain useful trends with respect to the cluster size after using a quantitative framework to compare and classify the chirality of TPGC? These questions were addressed in 2015, and after a systematic calculation of the HCM for ~26 TPGC in the size range of 18–144 Au atoms, interesting and useful insights were obtained [77].

To quantify the chirality of a TPGC, it is useful to visualize its overall structure as a metal core covered by a protecting shell, as was proposed by the ‘divide and protect’ model [114]. This core–shell partition is also justified by the total structure determination obtained from the X-ray data in crystallized cluster samples [75]. A more precise description of the TPCG shows that the surface of its metal core interacts with a ligand shell that consists of ‘staple’ motifs of different length (see Section 2). This protecting shell interacting with the metal core surface is called the Au–S interface. The full cluster structure is completed by the remaining organic tail of the thiolate ligands. The HCM methodology can assign quantitative indexes to the chirality existing in TPGC, including those corresponding to the metal core, the Au–S interface, the organic tail, and the overall cluster structure [77]. The main trend obtained from the calculated HCM values of TPGC across the size range of 18–144 Au atoms shows that the Au–S interface has the dominant contribution to the overall cluster chirality [77]. For example, most of the chiral clusters investigated can be described as an achiral or ‘weakly’ chiral metal core protected by a ligand shell displaying a chiral Au–S interface. Figure 5 shows the structure and HCM values for two of the most well-known chiral $\text{Au}_{38}(\text{SR})_{24}$ [93,94] and $\text{Au}_{102}(\text{SR})_{44}$ [92] clusters, corresponding to this classification. On the other hand, the HCM methodology has been also useful to identify clusters where the metal core displays a strong chirality. The phosphine-protected Au_{20} gold cluster [115,116], as well as the thiolate-protected Au_{44} [117], Au_{52} [117], and Au_{133} [118,119] clusters belong to this category, corresponding to cases in which the overall chirality is concentrated in the metal core. Figure 6 displays the cluster structures and HCM values of the thiolate-protected Au_{44} and Au_{52} clusters which have metal cores with the highest HCM values. On the other hand, Figure 7 shows the HCM indexes calculated for most of the TPGC known up to 2015 [77], displaying the values for the whole protected cluster (yellow triangles) in an ascending order. It was also obtained that 5 out of 26 clusters are achiral ($\text{HCM} < 0.001$). Figure 7 also indicates that for most cases the HCM values calculated for the ligand arrangement forming the protecting shell (red diamonds) are very similar to those of the whole cluster, but the core values (blue squares) are smaller. These results indicate that in general, chirality is mainly due to the chiral arrangement of ligands, although interesting exceptions have been found where the metal cores have large HCM values.

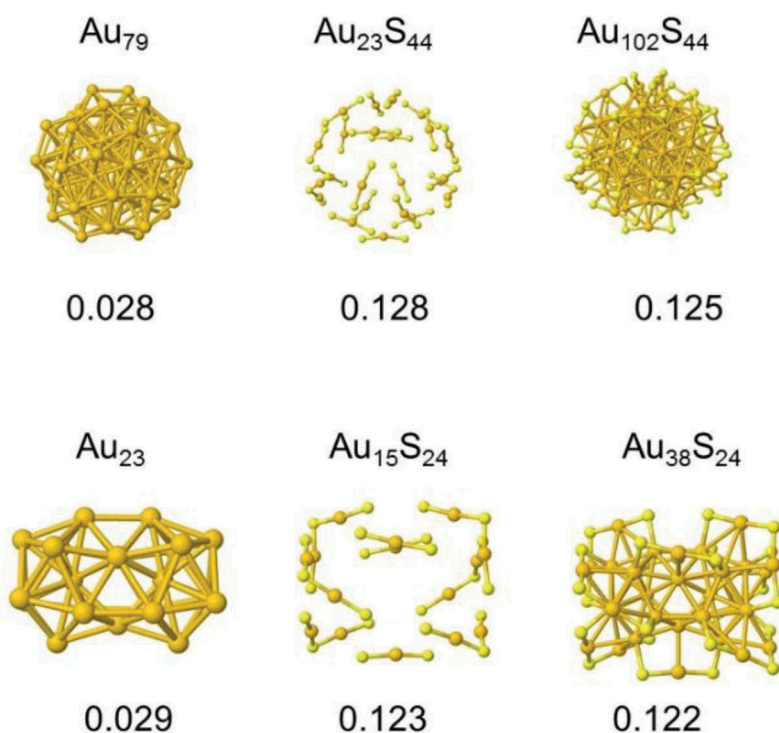


Figure 5. Structures and HCM values for the cluster core, ligand shell (Au–S interface), and protected cluster. Top panel: $\text{Au}_{102}(\text{SR})_{44}$; bottom panel: $\text{Au}_{38}(\text{SR})_{24}$. Au atoms are in dark yellow and S are in light yellow. This figure is adapted from the original one reported in Ref. [77].

The results obtained by quantifying chirality using the HCM methodology are consistent with those obtained from symmetry considerations and are reliable to extract trends on how chirality is spatially distributed on the whole structure of the TPGC [77]. However, further investigations are required to validate this approach through the search of systematic and clear correlations between the HCM values and physical and/or chemical manifestations of chirality like the optical activity (CD spectrum), or the strength of enantiomer-specific interactions between TPGC and other chiral systems [120–122]. The existence of these correlations is discussed in Section 5.

4. First-principles calculation of the CD spectrum

In molecular physics, there are many methods available to calculate the electronic structure of molecules and their optical properties. However, such methods are often computationally too demanding to be applied in practice to large systems like nanoclusters. Moreover, if one is interested in

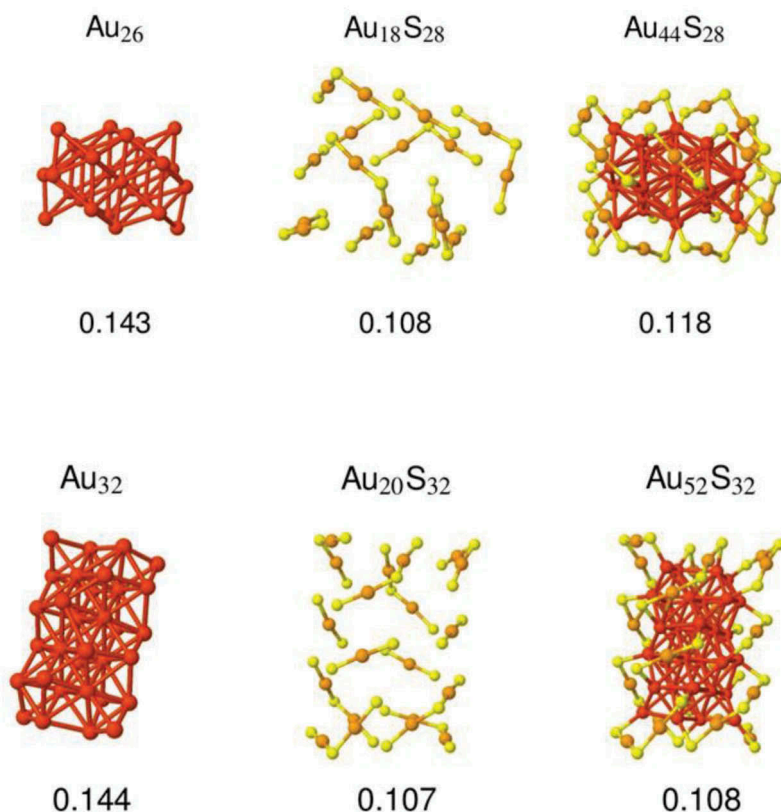


Figure 6. Structures and HCM values for the cluster core, ligand shell (Au–S interface), and protected cluster. Top panel: $\text{Au}_{44}(\text{SR})_{28}$; bottom panel: $\text{Au}_{52}(\text{SR})_{32}$. Core Au atoms are in red, shell Au atoms are in dark yellow, and S are in light yellow. This figure is adapted from the original one reported in Ref. [77].

the CD, the molecule under study must be chiral and therefore with very low or even without any symmetry, rendering the computation even more heavy. Keeping this situation in mind, it is obvious that very accurate (correlated) *ab-initio* methods cannot be applied in this field, and the only practicable schemes are the density functional theory (DFT) and its time-dependent extension (TDDFT). The first TDDFT implementation to calculate the CD has been introduced by Autschbach and Ziegler [123,124]. In that implementation, the TDDFT equations were solved according to the Casida's scheme [125] which consists of the diagonalization of a matrix, whose dimension is the product of the number of the occupied orbitals times the number of virtual orbitals. This method is very efficient when only the lowest part of the spectrum is needed, a situation which is not standard for nanoclusters. For this reason, a new TDDFT algorithm, which extracts the spectrum from the imaginary part of the complex

Hausdorff chirality measure of ligand-protected gold clusters

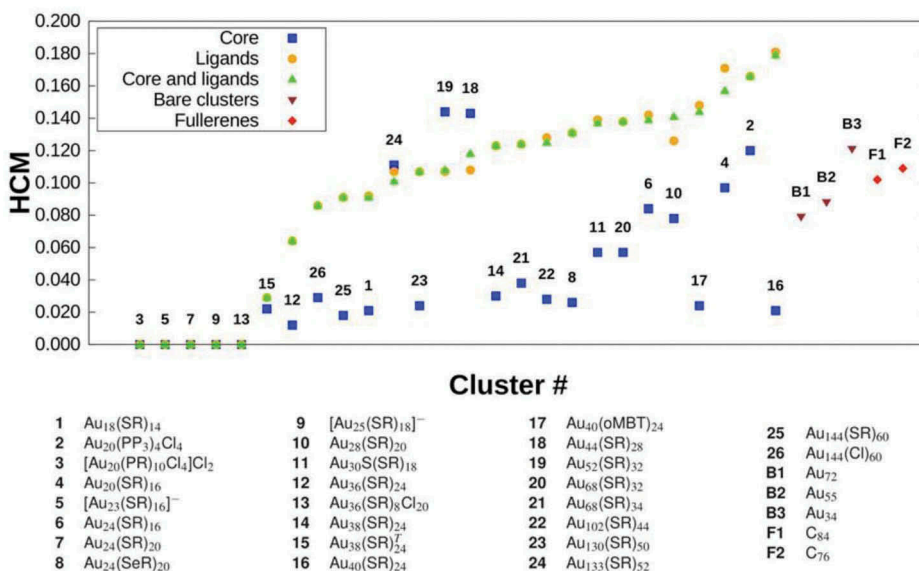


Figure 7. HCM index of chirality for ligand-protected gold clusters. The numbers in black above the blue squares denote the cluster number according to the list shown in the bottom panel. This figure is adapted from the original one reported in Ref. [77].

polarizability, has been implemented recently [126] and extended for the calculation of the CD spectrum [127].

4.1. The complex polarizability method

To describe the complex polarizability method, we briefly resume the basic theory of CD. For a molecule with fixed orientation, the CD of an electronic transition from the ground state $|0\rangle$ to the n th excited state $|n\rangle$ corresponds to the difference between the absorbance of left and right circularly polarized light which propagates along the X -direction as follows [128]:

$$CD = A_L - A_R = 2\gamma \text{Im}(\langle 0 | \mu_Y | n \rangle \langle n | m_Y | 0 \rangle + \langle 0 | \mu_Z | n \rangle \langle n | m_Z | 0 \rangle), \quad (1)$$

where in Equation (1) μ and m are the electric dipole and magnetic dipole moment operators, respectively, and γ is a constant.

In solution or in the gas phase, molecules are randomly oriented, so Equation (1) must be rotationally averaged, and the Rosenfeld equation is obtained as follows:

$$CD = \frac{4}{3} \gamma \text{Im}(\langle 0|\mu|n\rangle \cdot \langle n|\mathbf{m}|0\rangle) \quad (2)$$

The rotatory strength, R_{0n} , is therefore defined as follows:

$$R_{0n} = \text{Im}(\langle 0|\mu|n\rangle \cdot \langle n|\mathbf{m}|0\rangle) \quad (3)$$

To calculate R_{0n} by means of the complex polarizability algorithm [127], it is convenient to consider the dipole moment induced by an electromagnetic field [129]:

$$\mu'_u = \sum_v \alpha_{uv} E_v - \sum_v \frac{\beta_{uv}}{c} \frac{\partial B_v}{\partial t}. \quad (4)$$

In Equation (4), E_v and B_v are the electric and magnetic field components, c is the speed of light, α is the dynamical polarizability tensor, and β is the optical rotation tensor which is related to the rotatory strength by the following sum over states expression:

$$\bar{\beta} = \frac{1}{3} \sum_u \beta_{uu} = \frac{2c}{3} \sum_n \frac{R_{0n}}{\omega_{0n}^2 - \omega^2} \quad (5)$$

In Equation (5), ω is the photon energy and ω_{0n} corresponds to the $|0\rangle \rightarrow |n\rangle$ excitation energy. Therefore, it is convenient to extract R_{0n} from the β imaginary part as in conventional photoabsorption. From Equation (4), β consists of the electric dipole moment induced by a time-dependent magnetic field and can be calculated by the following expression:

$$\beta_{zz}(\omega) = \left(-\frac{ic}{\omega} \right) \sum_i^{\text{occ}} \sum_a^{\text{virt}} \langle \phi_i | m_z | \phi_a \rangle \bar{P}_i^a \quad (6)$$

with

$$\bar{P}_i^a = t_k(\omega) \left[\langle \phi_a | \mu_z | \phi_i \rangle + \sum_{\mu\tau}^{\text{fit}} (A^k)_{ia,\mu}^+ L_{\mu\tau} b_\tau \right] \quad (7)$$

In Equations (6) and (7), the $A_{\mu,ia}^k$ are integrals between the auxiliary fitting function f_μ and the product between the i th occupied and the a th virtual orbitals, $\langle \phi_i | \mu_z | \phi_a \rangle$ and $\langle \phi_i | m_z | \phi_a \rangle$ are the electric and magnetic dipole moment matrix elements, respectively, between the same occupied-virtual (ia) orbitals pair, the matrix \mathbf{L} is defined by Equation (28) in Ref. [126], t_k is given by

$$t_k(\omega) = \frac{1}{\omega - \omega_{0n} + i\varepsilon} + \frac{1}{\omega + \omega_{0n} + i\varepsilon} \quad (8)$$

and \mathbf{b} is the solution of the following linear system:

$$[\mathbf{S} - \mathbf{M}(\omega)]\mathbf{b} = \mathbf{d} \quad (9)$$

In practice, the resolution of the TDDFT equations is recast to the linear system (9) (see Ref. [126]. for a detailed description), which is already solved to calculate the photoabsorption, so the CD calculation is computationally irrelevant. It is worth noting that the linear system (9) is solved employing the auxiliary density fitting functions as a basis set to represent vectors and matrixes. This means that the dimension of Equation (9) is much lower with respect to the Casida's approach.

Equation (9) is then solved point by point for each photon energy; moreover, the real photon energy is supplemented with a small imaginary part. This procedure generates a Lorentzian broadening of the discrete transition.

It is worth mentioning that for CD calculations, the rotatory strength (R) is invariant under molecular translations only if the electric dipole elements are calculated within the velocity gauge. In practice, one must use in Equation (7) the following form of the dipole matrix elements:

$$\langle \phi_a | \mu_z | \phi_i \rangle = \frac{\langle \phi_a | \frac{d}{dz} | \phi_i \rangle}{\varepsilon_a - \varepsilon_i} \quad (10)$$

As discussed above, CD spectra correspond to a linear response calculation. They therefore need a higher-quality basis set with respect to ground-state DFT calculations to achieve a comparable accuracy. A rigorous way to check that the basis set employed in any given case is of sufficient quality is to compare CD spectra calculated in the length and velocity gauge, which should coincide at the basis set limit. For typical nanoclusters and sufficiently high-quality basis set [127], we found negligible differences between the length and the velocity gauge, so when using an appropriate computational numerical setup, R can be safely calculated employing the standard-length gauge of the electric dipole moment.

4.2. Fragment projection analysis of the CD spectra

Chirality is a complex phenomenon and is often difficult to get meaningful physical insights into it. In this situation, the analysis tools of TDDFT CD spectra can be potentially useful to shed light on chirality and try to understand its origin in any given system, especially in multifunctional composite systems such as thiolate-protected metal nanoclusters, exhibiting excitations mixing electronic states from metal, sulphur, and organic-residue atoms. This is interesting from both a fundamental point of view and also in practical applications, as it can open avenues to a more precise control and exploitation of this complex phenomenon. To this purpose, here we extend to CD a fragment projection analysis, originally developed

for photoabsorption [130], based on the fragment projection of electronic excited states and on induced transition densities. The aim of this analysis tool is to rationalize the interplay among excitations belonging to the metal cluster and coating shell in determining the dichroism of metal nanoclusters, and to achieve it by dissecting the system into two pieces or fragments that will be named M and L for convenience, and to express the CD as a sum of four terms, corresponding to $M \rightarrow M$, $M \rightarrow L$, $L \rightarrow M$, $L \rightarrow L$ transitions.

We start with the expression of the rotatory strength as calculated with the complex polarizability algorithm:

$$R = \frac{3\varepsilon\omega}{2c} \text{Im}(\bar{\beta}) \quad (11)$$

In Equation (11), ω is the photon energy, c is the speed of light, ε is the HWHM of the electronic transition, which corresponds to the imaginary part of the frequency, and $\bar{\beta}$ stands for the averaged optical rotation tensor whose diagonal elements are given by Equation (6). In Equation (6), a double sum over occupied and virtual orbitals involves a product of a magnetic dipole matrix element between a pair of occupied-virtual orbitals and a density matrix element, \bar{P}_i^a , between the same occupied-virtual orbital pair, which is calculated as detailed in Ref. [127]. In practice, we aim at splitting each term of the sum in Equation (6), related to a given occupied-virtual pair, into four contributions $M \rightarrow M$, $M \rightarrow L$, $L \rightarrow M$, $L \rightarrow L$ according to the weights of the fragment in the occupied and virtual orbitals. Here, we consider a simplified fragment projection, performed in terms of the Mulliken analysis of the corresponding molecular orbitals (in future work we will consider more sophisticated fragment decomposition analyses). We thus make use of the normalization condition:

$$1 = \sum_{\lambda\mu} C_{i\lambda} + S_{\lambda\mu} C_{\mu i} = \sum_{\mu} M_{\mu i} = \sum_F \sum_{\mu \in F} M_{\mu i} = \sum_F M_{Fi} \quad (12)$$

$$M_{\mu i} = \sum_{\lambda} C_{i\lambda}^+ S_{\lambda\mu} C_{\mu i} \quad (13)$$

$$M_{Fi} = \sum_{\mu \in F} M_{\mu i} \quad (14)$$

where in Equations (12–14) λ, μ are indexes running over the basis set, $C_{\mu i}$ are the coefficients of the orbital i onto the basis functions μ , $S_{\lambda\mu}$ are the elements of the overlap matrix, and F is an index running over fragments (M and L in the present case of only two fragments). Now, we insert in

Equation (6) two further sums over fragments as in the last term of Equation (12):

$$\beta_{zz}(\omega) = \left(-\frac{ic}{\omega}\right) \sum_i^{occ} \sum_a^{virt} \langle \phi_i | m_z | \phi_a \rangle \bar{P}_i^a \sum_F M_{Fi} \sum_G M_{Ga} \quad (15)$$

Equation (15) can thus be finally rewritten as follows:

$$\beta_{zz}(\omega) = \left(-\frac{ic}{\omega}\right) \sum_F \sum_G CD_{FG} \quad (16)$$

where

$$CD_{FG} = \sum_i^{occ} \sum_a^{virt} \langle \phi_i | m_z | \phi_a \rangle \bar{P}_i^a M_{Fi} M_{Ga} \quad (17)$$

therefore, achieving the desired splitting into fragment contributions of the energy-dependent optical rotation tensor elements.

4.3. Individual component maps of rotatory strength (ICM-RS) analysis

Recently, an analysis tool of the absorption spectra derived from TDDFT simulation has been proposed, i.e. individual component maps of oscillatory strength (ICM-OS) plots [131], which allows one to investigate the connection between absorption and single-particle excitations (ICM-OS). The theory behind ICM-OS is very simple. We start from the oscillator strength at each given frequency (z -component) calculated as the imaginary part of the zz diagonal element of the dynamical polarizability tensor:

$$\alpha_{zz}(\omega) = \sum_i^{occ} \sum_a^{virt} \langle \phi_i | z | \phi_a \rangle P_i^a(z) \quad (18)$$

where P_i^a is a density matrix element due to the electric field in the Z -direction and $\langle \phi_i | z | \phi_a \rangle$ is a dipole matrix element, both evaluated over a pair of occupied(=i)/virtual(=a) single-particle molecular orbitals. As ICM-OS(ω), we then plot the individual $\langle \phi_i | z | \phi_a \rangle P_i^a$ components as functions of the single-particle energies of occupied (ε_i) and virtual (ε_a) orbitals. The optical absorption intensity at each given energy is proportional to the integral of the ICM-OS(ω) at the given energy over the ($\varepsilon_i, \varepsilon_a$) plane, and the individual peaks are smeared with a Gaussian function to make them visually clearer. As demonstrated in Ref. [131], the positive and negative components of the ICM-OS plots allow one to clarify both the nature of the excited state and also the relative sign of the contribution of the dipole versus density matrix elements on the oscillator strength, and thus to single out destructive interference effects. In an entirely analogous

way, we can define ICM-RS plots as analysis tools of chiro-optical linear response spectra derived from TDDFT. We start from the rotatory strength at each given frequency (z -component) calculated as the imaginary part of the zz diagonal element of the circular dichroic tensor [127]:

$$CD_z(\omega) = -\frac{3\varepsilon}{2} \text{Re} \left(\sum_i^{\text{occ}} \sum_a^{\text{virt}} \langle \phi_i | m_z | \phi_a \rangle \bar{P}_i^a[z] \right) \quad (19)$$

where in Equation (19) ε corresponds to the Lorentzian energy broadening, $\bar{P}_i^a[z]$ is the density matrix element given by Equation (7), due to the perturbation induced by the z -component of the electric dipole, and $\langle \phi_i | m_z | \phi_a \rangle$ is a matrix element of the magnetic dipole over a pair of occupied/virtual single-particle molecular orbitals. As in the case of ICM-RS(ω), we then plot the individual $\langle \phi_i | m_z | \phi_a \rangle \bar{P}_i^a[z]$ components as functions of the single-particle energies of occupied (ε_i) and virtual (ε_a) orbitals. The ICM-RS(ω) plots allow one to visualize the source of chiral response in momentum space, including signed contributions and therefore highlighting cancellation terms that are ubiquitous in chiral phenomena. Indeed, in Ref. [132], ICM-RS plots have been proposed and discussed in detail to analyse the chiro-optical spectra of a series of (Ag–Au)₃₀(SR)₁₈ TPGC, finding that these can be broadly classified as of whether destructive interference and cancellation in their chiro-optical response arise from occupied–virtual orbital pair contributions corresponding to orbitals with similar or dissimilar excitation energies. Further developments along this avenue will be reported in future work.

5. Correlation between the geometric quantification of chirality and chiroptical measurements

In Section 3, we discussed the convenience and advantages of quantifying the chirality existing in TPGC from a geometrical point of view. To this purpose, the methodology based on HCM had been used in the literature to assign and compare the index of chirality of the cluster core, protecting shell, and overall cluster structure of TPGC in the size range of 18–144 Au atoms [77]. Interesting trends as well as useful insights on the origin of chirality were obtained, resulting that for most of the TPGC, the Au-S interface plays the key role for the chiral cluster behaviour [77]. In this section, we will present and discuss useful results to investigate the existence of a correlation between the geometrical measure of chirality and the chiroptical response of chiral bare gold clusters and TPGC. This correlation will be useful not only to further validate the proposal of geometrically quantifying the chirality of such compounds, but also to gain new insights

into the mechanisms responsible of the complex peak structure in the lineshape of the CD spectra.

There had been several studies that investigated the existence of a correlation between geometrical indicators of chirality and the chiroptical activity displayed by different types of chiral nanomaterials. In 2014, an experimental report on the detection, visualization, and measurement of chirality in gold NPs using helical pitch measurements for the transfer of chirality into nematic liquid crystal phases was published [133]. Another study examined the evolution of the theoretically calculated CD spectra with geometrical parameters such as bond and dihedral angles for neutral silver nanowires of helical shape [134]. This study indicated that the intensity of the CD peaks is strongly affected by the shape of the helix [134]. A more recent theoretical-experimental investigation of the chiroptical response of sigmoidal gold clusters revealed that the strong CD responses are closely related to the metal electronic orbitals, thus correlating the CD response with the geometrical (sigmoidal) arrangement of gold atoms [135]. The first attempt to correlate HCM values with optical activity measurements was reported in 2016 using two small Au₈ and Au₁₁ gold clusters protected by chiral diphosphines [136]. Although a quantitative correlation between the HCM values and the CD overall intensity profile of these compounds was not found, it is worthwhile and necessary to perform additional tests looking for the existence of such correlation in larger chiral gold clusters.

In the following, we will present additional examples of the search for a correlation between HCM values and the CD intensity profile of chiral bare Au clusters and chiral TPGC. The first example corresponds to the chiral anionic bare cluster Au₃₄⁻, which has been experimentally and theoretically investigated since 2007 [102–104]. This cluster with C₃ point symmetry can be considered as a representative example of bare chiral gold clusters, since it corresponds to the lowest-energy isomer in the potential energy surface of Au₃₄⁻ [102,104]. Its C₃ chiral symmetry appears after performing the rotation of the hexagonal facets forming the surface of the related C_{3v} isomer, which correspond to a 34-atom cluster fragment of an fcc lattice. **Figure 8** shows the chiral transformation between the C_{3v} and C₃ isomers along with eight intermediate structures, with the rotation of the hexagonal facets highlighted in red. The HCM value for each structure is also shown, indicating a monotonically increase with the rotational angle of the facets, starting at HCM = 0.000 for the achiral C_{3v} isomer and ending with the maximum HCM = 0.120 value for the chiral C₃ isomer. The structures of the 10 clusters shown in **Figure 8** were used to calculate the CD spectra using the TDDFT methodology discussed in **Section 4**. Specifically, a scalar relativistic pseudopotential with 19 valence electrons, the LAN2DZ basis set, the PBE xc functional, and 200 excited

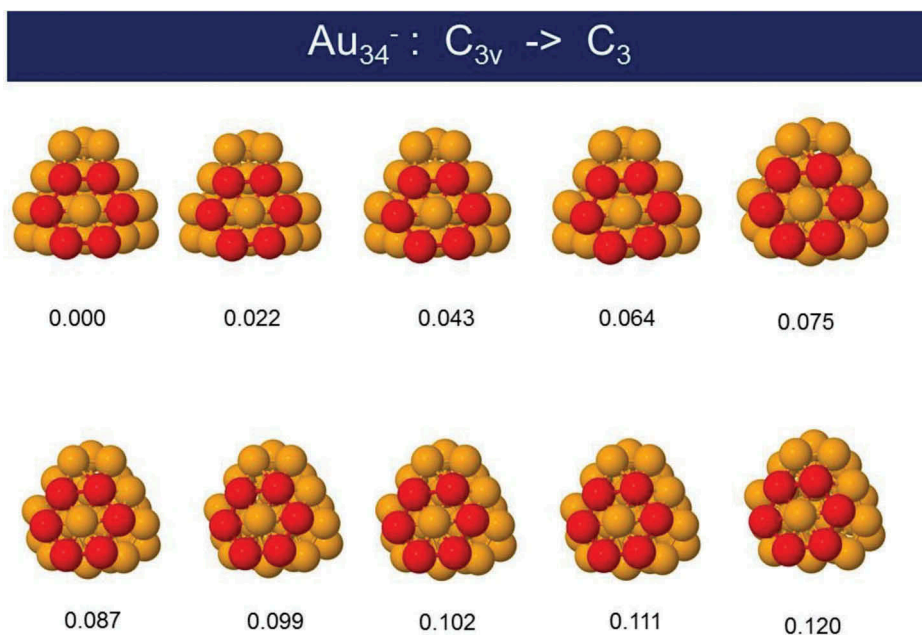


Figure 8. Structures and HCM values for the Au_{34}^- anionic cluster. The cluster on the left-upper corner corresponds to the achiral C_{3v} isomer with a zero HCM value. The cluster at the right-bottom corner is the chiral C_3 isomer with the maximum HCM = 0.120 value. The other clusters have intermediate structures between the C_{3v} and C_3 isomers. They were obtained from the relative rotation of the hexagonal facets highlighted in red. Their intermediate HCM values are also shown.

states as implemented in the Gaussian09 code [137], were utilized to calculate the CD spectra displayed in Figure 9. The calculated CD spectra were separated in three sets according to their intensity profile: weak, medium, and strong. This classification is in good correlation with the increasing HCM values shown in Figures 8 and 9. In fact, the lineshape of the CD spectra evolves from zero intensity for the achiral C_{3v} isomer with HCM = 0.000, to weak intensity for the structures with small HCM values, to higher intensity for structures with larger HCM values, up to the maximum intensity profile obtained for the C_3 chiral isomer. This HCM–CD correlation is more evident for the negative and positive peaks in the low-energy range between 0.5 and 2.0 eV, where the transitions are between states near the HOMO–LUMO gap, corresponding to both intra-band ($sp \leftarrow sp$) and interband ($sp \leftarrow sp$, $sp \leftarrow d$) transitions [104].

For TPGC, Figure 10 shows a good qualitative correlation between the HCM values and the calculated CD lineshape of the $\text{Au}_{18}(\text{SCH}_3)_{14}$, $[\text{Au}_{25}(\text{SCH}_3)_{18}]^-$, and $\text{Au}_{38}(\text{SCH}_3)_{24}$ thiolate-protected gold clusters. In these cases, the CD spectra were calculated using the TDDFT methodology as implemented in the Gaussian09 [137] code with 200 excited states, a scalar relativistic pseudopotential with 19 valence electrons described through the LAN2DZ basis set for the Au

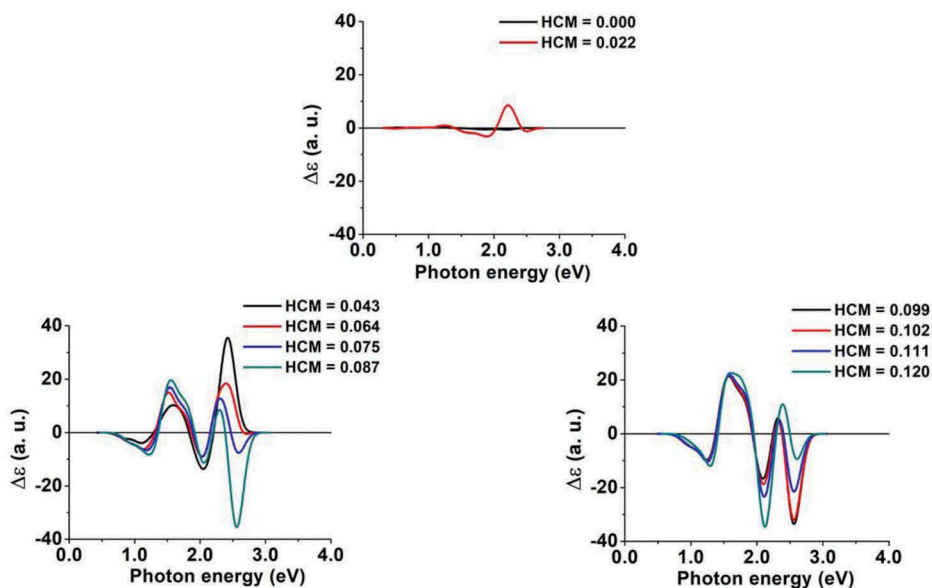


Figure 9. Calculated circular dichroism spectra of the 10 Au_{34}^- cluster structures displayed in Figure 8.

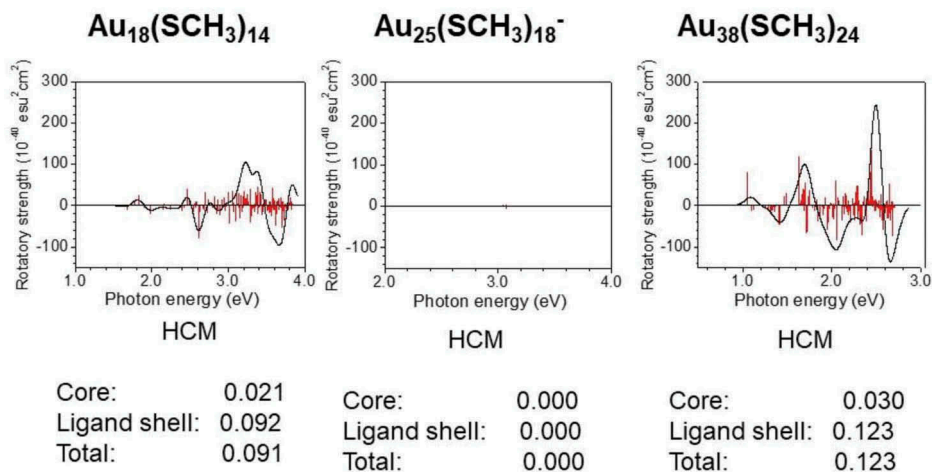


Figure 10. Calculated rotatory strength and HCM index of chirality for ligand-protected gold clusters. The overall intensity lineshape correlates well with the HCM values.

atoms, an all-electron description with a 6-31G(d,p) basis set for the S, C and H atoms, and the PBE xc functional. The cluster structures were obtained by a relaxation of the xyz Cartesian coordinates taken from the XRC data measured for such thiolate-protected clusters [93,138,139]. In Figure 10, it can be appreciated that, as expected, the CD spectrum is null for the achiral $[\text{Au}_{25}(\text{SCH}_3)_{18}]^-$ cluster, whereas for $\text{Au}_{18}(\text{SCH}_3)_{14}$, with relatively small HCM values, the CD lineshape shows a rotatory strength with a limited variation in the range between

100 and $-100 \times 10^{-40} \text{ esu}^2\text{cm}^2$. In contrast, the overall intensity change of the rotatory strength is higher for the $\text{Au}_{38}(\text{SCH}_3)_{24}$ cluster in the range between 250 and $-140 \times 10^{-40} \text{ esu}^2\text{cm}^2$, which is consistent with its larger HCM values.

To further explore the correlation between the geometric index of chirality HCM with the CD spectrum, a set of four related chiral TPGC recently synthesized and crystallized were considered. They are $\text{Au}_{28}(\text{TBBT})_{20}$, $\text{Au}_{36}(\text{TBBT})_{24}$, $\text{Au}_{44}(\text{TBBT})_{28}$, and $\text{Au}_{52}(\text{TBBT})_{32}$ (TBBT: 4-tert-butylbenzenethiolate). Utilizing the atomic coordinates extracted from the XRC data, the HCM values were calculated [77]. They are displayed in Figure 11 along with the cluster structures. In these cases, the overall cluster structure was divided into an inner metal core, a shell(i) formed by the Au-S interface, and a shell(ii) that, in addition to the Au-S interface, also includes the benzene carbon rings (C_6), which is the nearest organic group to the S atom of the TBBT ligand. Figure 11 shows the calculated HCM values for the metal core, shell(i), shell(ii), core + shell(i), and core + shell(ii). These values are useful not only to compare the contributions of the core and Au-S interface as was done before, but also to know the contribution of the organic part of the ligand. Interesting trends can be obtained by comparing these values. For example, the HCM values for the metal core are relatively large, except for the Au_{20} core of the $\text{Au}_{36}(\text{SC}_6)_{24}$ protected cluster. Nevertheless, looking at the last column of the table shown in Figure 11 with the HCM values of the overall cluster structure (core + shell(ii)), it is obtained that all clusters would have large indexes of chirality, with the value for the $\text{Au}_{28}(\text{SC}_6)_{20}$ being slightly larger. This behaviour can be explained by

Cluster	Core	Shell (i)	Shell (ii)	Core + Shell (i)	Core + Shell (ii)
$\text{Au}_{28}(\text{SC}_6)_{20}$	Au_{14} 0.201	$\text{Au}_{14}\text{S}_{20}$ 0.140	$\text{Au}_{14}(\text{SC}_6)_{20}$ 0.142	$\text{Au}_{28}\text{S}_{20}$ 0.144	$\text{Au}_{28}(\text{SC}_6)_{20}$ 0.146
$\text{Au}_{36}(\text{SC}_6)_{24}$	Au_{20} 0.013	$\text{Au}_{16}\text{S}_{24}$ 0.064	$\text{Au}_{16}(\text{SC}_6)_{24}$ 0.124	$\text{Au}_{36}\text{S}_{24}$ 0.064	$\text{Au}_{36}(\text{SC}_6)_{24}$ 0.124
$\text{Au}_{44}(\text{SC}_6)_{28}$	Au_{26} 0.156	$\text{Au}_{18}\text{S}_{28}$ 0.119	$\text{Au}_{18}(\text{SC}_6)_{28}$ 0.122	$\text{Au}_{44}\text{S}_{28}$ 0.118	$\text{Au}_{44}(\text{SC}_6)_{28}$ 0.123
$\text{Au}_{52}(\text{SC}_6)_{32}$	Au_{32} 0.154	$\text{Au}_{20}\text{S}_{32}$ 0.105	$\text{Au}_{20}(\text{SC}_6)_{32}$ 0.117	$\text{Au}_{52}\text{S}_{32}$ 0.105	$\text{Au}_{52}(\text{SC}_6)_{32}$ 0.117

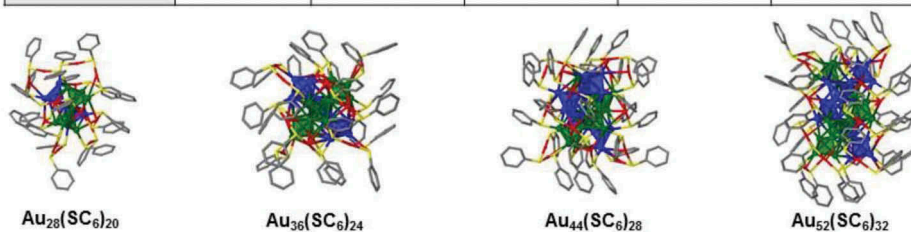


Figure 11. Calculated HCM values and structures of $\text{Au}_n(\text{SC}_6)_m$ clusters.

noticing that the HCM values calculated for the shell(ii) includes the contribution of the organic part of the ligands. These HCM values are large, as those calculated for the overall cluster structure.

One interesting question in this investigation is whether the above trends displayed by the HCM values correlate well with the chiroptical response. To start answering this question, it is interesting at this point to contrast the HCM predictions with both the total TDDFT response and a fragment-projection analysis of the TDDFT CD spectra, obtained via TDDFT/LB94 simulations using the complex polarizability method detailed in [Section 4](#). Fragment-projection has also been introduced in [Section 4](#), to which we refer for its methodological description. The calculations have been conducted on the species: $\text{Au}_{28}(\text{SPh})_{20}$, $\text{Au}_{36}(\text{SPh})_{24}$, $\text{Au}_{44}(\text{SPh})_{28}$, and $\text{Au}_{52}(\text{SPh})_{32}$, in which the TBBT ligand is simplified to a phenyl thiolate SPh for reducing the computational effort. The first point of a fragment analysis is to define how the atoms of the systems are partitioned into the two (M and L) fragments. In this work, we select as fragment M: all S and Au atoms (including those in the staples), and as fragment L: the phenyl residues, i.e. $(M//L) \equiv (\text{Au}, \text{S} // \text{C}, \text{H})$.

We report in [Figure 11](#) the HCM predictions, and in [Figure 12](#) the TDDFT-calculated CD spectra of the four compounds investigated here (black full line) and their fragment decomposition (coloured dotted lines, red = M→M, green = M→L, yellow = L→M, blue = L→L contributions). From an inspection of [Figure 12](#), we immediately draw that for a proper comparison between the HCM and the fragment analysis, we must focus on the optical region of the spectrum (excitation energies ≤ 3 eV) and neglect the UV region (>3 eV roughly): the reason for this is that in the UV region the CD response is dominated by a severe cancellation among the various M→M, M→L, L→M, L→L contributions, so that a comparison with purely geometrical quantities become less meaningful. The HCM values seem to compare reasonably well with the overall appearance of the CD spectra below 3 eV. In making this comparison, it should be recalled that the HCM values are normalized by the cluster size, using the largest interatomic distance in the cluster (see [Appendix A](#)), whereas the CD spectra report the absolute intensity of the rotatory power: this normalization clearly favours the smaller species with respect to the larger ones, and should be discounted in a proper match. Taking the size normalization of HCM values into account, one can see a semi-quantitative correlation between the HCM and the CD spectra, with a minimum in the predicted rotatory strength for $\text{Au}_{36}(\text{SPh})_{24}$ in both HCM and TDDFT values.

When coming to the fragment analysis of the TDDFT CD spectra, the first point to be noted in [Figure 12](#) is that the L→L contributions are usually small in the optical region. Their sizes are not completely negligible, but they tend to be minor with respect to the other components. This is in good agreement with a comparison of the last two columns in [Figure 11](#), i.e. core + shell(i) and core + shell(ii), which similarly shows that

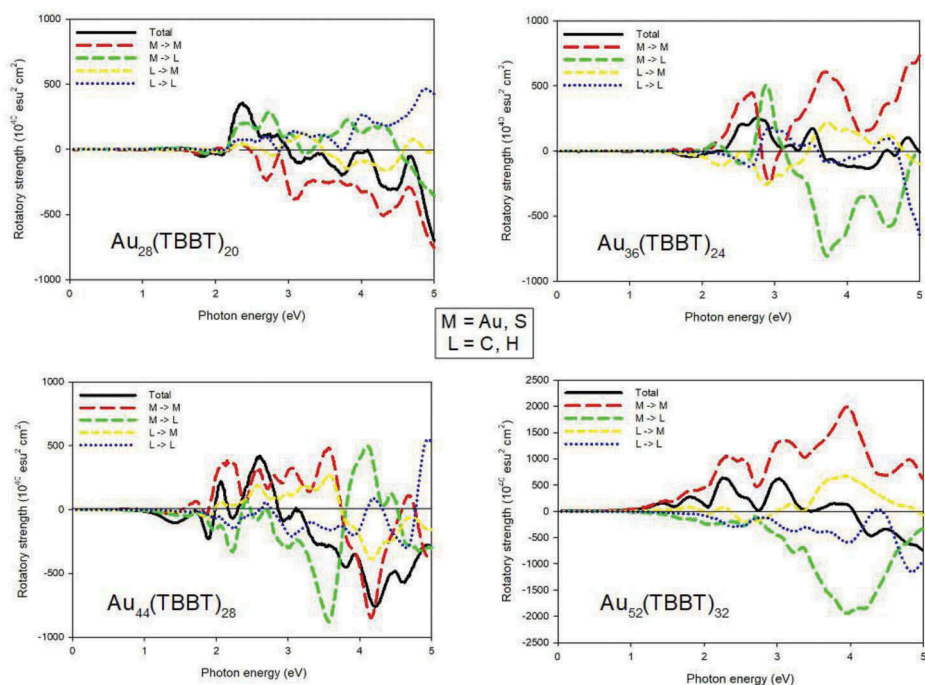


Figure 12. Total and fragment analysis CD spectra of $Au_n(TBBT)_m$ clusters. The colour coding for the dotted lines representing the fragment decomposition contributions is as follows: red = M→M, green = M→L, yellow = L→M, blue = L→L contributions.

the contribution of the C_6 groups to HCM values is usually minor: very small for $Au_{28}(TBBT)_{20}$, intermediate and increasing with size for $Au_{44}(TBBT)_{28}$ and $Au_{52}(TBBT)_{32}$, and only important for $Au_{36}(TBBT)_{24}$, a cluster for which it roughly doubles the HCM value. This compares well with Figure 12 (attention should be paid to the different scales of the ordinate axis), in which the maximum of the dotted blue curves in the optical region follows the order: $Au_{28}(TBBT)_{20} < Au_{44}(TBBT)_{28} \approx Au_{36}(TBBT)_{24} < Au_{52}(TBBT)_{32}$. It should be also noted that the excitations of $Au_{36}(TBBT)_{24}$ involving the phenyl residues increase the CD response close to 3 eV, which may be correlated with the increase predicted at the HCM level.

The second point to be noted in Figure 12 is that the M→M contributions become progressively dominant with an increasing size of the cluster. A more detailed analysis (not reported here) shows that the most important excitations are from the electronic states in the Au(staples)-S shell into the states localized within the Au core for the larger clusters in particular for $Au_{52}(TBBT)_{32}$, whereas for $Au_{28}(TBBT)_{20}$ the most important excitations are only localized in the Au(staples)-S shell. Therefore, the comparison of the fragment analysis with the HCM values is good for the larger clusters, fair for $Au_{36}(TBBT)_{24}$, for which the TDDFT analysis shows a transitional behaviour with a strong

cancellation of different contributions, whereas it is less good for the smallest cluster of the series, i.e. $\text{Au}_{28}(\text{TBBT})_{20}$. Specifically, the large HCM value predicted for the Au_{14} core for this smallest cluster, even after discounted the HCM normalization by its largest interatomic distance, does not find a correspondence in the fragment analysis, which exhibits that the CD spectrum should be dominated by the $\text{Au}(\text{staples})\text{-S} \rightarrow \text{Au}(\text{staples})\text{-S}$ excitations. The reason of this discrepancy is probably due to the fact that the excitations from this small metal core go to high energies and are not correctly predicted by a geometrical model.

As a general conclusion for this brief comparison, we can say that the purely geometrical HCM analysis proves to be qualitatively correct, especially considering its simplicity, however only when it is limited to the optical region of the CD spectra and focuses on the larger rather than on the small clusters. Future developments and improvements may entail convoluting the HCM with some form of weight of the CD intensity to make it more predictive. The examples discussed above, showing a good correlation between the HCM values and the lineshape of the CD spectra, are encouraging towards the validation and usefulness of quantifying and classifying the chirality of bare and TPGC using a geometrical measure.

6. Summary and perspectives

The main research results on the discovery, understanding, and physicochemical manifestations of chirality in bare and TPGC obtained during the last 20 years have been briefly revised. The initial discussion was dedicated to place in perspective the chirality in nanoclusters by describing it as a property that exists in a broad range of scales going from the molecular level to the nanoscale and even to larger chiral galactic systems. Chiral metal nanoclusters, bare and ligand-protected, were identified as a special and interesting kind of novel chiral nanomaterials, for which a huge research activity has been performed during the last two decades. In addition to the size and shape dependence of their physical and chemical properties, the chiral behaviour of these systems provides additional interest and complexity for their study. Useful insights and trends on the origin of this property, mainly based in the total structure determination by XRC, indicated that chirality could be intrinsic due to the stability of chiral patterns (mainly formed by achiral ligands) on the surface of a nearly symmetric metal core, or induced by chiral ligands that transfer chirality to the overall structure of the ligand-protected metal cluster. Moreover, the current view is that chirality could exist in the metal core, at the Au-S interface of the metal core and the ligand shell, and in the organic part (carbon tail) of the ligands.

An important contribution of this review was the discussion of the recent developments on two theoretical approaches to gain additional insights into the origin of chirality and the chiroptical response displayed by TPGC. In the first

approach, the proposal of quantifying chirality from a geometric point of view was discussed. In the second one, it was revised the first-principle methodology to calculate the CD spectra of thiolate-protected gold clusters of medium size from $\text{Au}_{18}(\text{SR})_{14}$ up to $\text{Au}_{52}(\text{SR})_{32}$. The use of these theoretical methodologies, based on the assignment of a numerical index of chirality, and in the quantum mechanical calculation of the chiroptical response of chiral bare and TPGC, clearly illustrates the way in which physics approaches the understanding of the complex phenomenon of chirality at the nanoscale. Moreover, the search for the correlation between these procedures exemplifies the capability of physics to connect the geometrical aspect of chirality with the optical response to the interaction between light (circularly polarized) and chiral nanomaterials. It is expected that this way of approaching chirality in bare and TPGC encourages alternative studies in which other disciplines, like chemistry, biology, or materials science, reveal additional knowledge towards gaining further understanding and promotion of technological developments of chiral nanomaterials.

Although great progress has been achieved in the study of chirality in bare and TPGC during the last 20 years, several remaining challenges still prevent us from reaching a full understanding of the phenomenon. From the experimental point of view, it is essential to develop more advanced methodologies for enantioseparation that allow to increase the number of enantiopure bare and TPGC and perform probes on the distinct chirality of these compounds. Additional techniques, besides chiral spectroscopies, are also necessary to characterize other manifestations of chirality like the chiral recognition between, for example, metal clusters and biological molecules [120–122]. At the theoretical level, the development of new measures of chirality, that consider not only the geometrical aspect but also the atomic and electronic properties like mass and charge distribution, is mandatory. Those novel methods to quantify chirality, once they get validated by their good correlation with physical and chemical manifestations of it, would be very useful to locate and design new chiral nanomaterials.

Acknowledgments

Calculations were performed at the DGTIC-UNAM Supercomputing Center under Project LANCAD-UNAM-DGTIC-049. I. L. Garzón thanks support from DGAPA-UNAM under Project IN108817 and Conacyt-Mexico under Project 285821. L. Chang is grateful to the China Scholarship Council for a scholarship supporting an internship at CNR-ICCOM. Support from CINECA supercomputing centre within the ISCR program is also gratefully acknowledged.

Disclosure statement

No potential conflict of interest was reported by the authors.

Funding

I. L. Garzón thanks support from DGAPA-UNAM under Project IN108817 and Conacyt-Mexico under Project 285821. L. Chang is grateful to the China Scholarship Council for a scholarship supporting an internship at CNR-ICCOM.

References

- [1] J.B. Biot. *Mém. Classe Sci. Math. Phys. Inst. Impérial France*. 2 (1812) p. 41
- [2] W.A. Bonner. *Origins Life Evolution Biospheres*. 21 (1991) p. 59
- [3] M.L. Pasteur. *Ann. Chim. Phys.* 24 (1848) p. 442
- [4] W.T.L. Kelvin, *Baltimore Lectures on Molecular Dynamics and the Wave Theory of Light*, Cambridge University Press, Cambridge, UK, 2010
- [5] G.H. Wagnière, *On Chirality and the Universal Asymmetry*, Verlag Helvetica Chimica Acta, Zürich, 2007
- [6] D.K. Kondepudi and D.J. Durand. *Chirality*. 13 (2001) p. 351. doi: [10.1002/chir.1044](https://doi.org/10.1002/chir.1044)
- [7] Z. Dogic and S. Fraden. *Phys. Rev. Lett.* 78 (1997) p. 2417. doi: [10.1103/PhysRevLett.78.2417](https://doi.org/10.1103/PhysRevLett.78.2417)
- [8] N. Berova, K. Nakanishi and R. Woodyeds. *Circular Dichroism: Principles and Applications*. John Wiley & Sons. USA, 2000
- [9] J. Kumar, K.G. Thomas and L.M. Liz-Marzán. *Chem. Commun.* 52 (2016) p. 12555. doi: [10.1039/C6CC05613J](https://doi.org/10.1039/C6CC05613J)
- [10] N. Berova, L. Di Bari and G. Pescitelli. *Chem. Soc. Rev.* 36 (2007) p. 914. doi: [10.1039/b515476f](https://doi.org/10.1039/b515476f)
- [11] T.A. Keiderling. *Appl. Spectrosc. Rev.* 17 (1981) p. 189. doi: [10.1080/05704928108060405](https://doi.org/10.1080/05704928108060405)
- [12] S. Liu, L. Han, Y. Duan, S. Asahina, O. Terasaki, Y. Cao, B. Liu, L. Ma, J. Zhang and S. Che. *Nat. Commun.* 3 (2012) p. 1215. doi: [10.1038/ncomms2215](https://doi.org/10.1038/ncomms2215)
- [13] S. Petoud, G. Muller, E.G. Moore, J. Xu, J. Sokolnicki, J.P. Riehl, U.N. Le, S.M. Cohen and K.N. Raymond. *J. Am. Chem. Soc.* 129 (2007) p. 77. doi: [10.1021/ja064902x](https://doi.org/10.1021/ja064902x)
- [14] K. Fauth, E. Goering, G. Schütz and L.T. Kuhn. *J. Appl. Phys.* 96 (2004) p. 399. doi: [10.1063/1.1759792](https://doi.org/10.1063/1.1759792)
- [15] P.L. Polavarapu, J. He, J. Crassous and K. Ruud. *Chem. Phys. Chem* (2005) p. 2535. doi: [10.1002/cphc.200500171](https://doi.org/10.1002/cphc.200500171)
- [16] K.W. Busch and M.A. Buscheds. *Chiral Analysis*. Elsevier. USA, 2011
- [17] A.N. Collins, N. Sheldrake and J. Crosbyeds. *Chirality in Industry II: Developments in the Commercial Manufacture and Applications of Optically Active Compounds. Vol. 2*. John Wiley & Sons. UK, 1997
- [18] W.A. Nugent, T.V. RajanBabu and M.J. Burk. *Science*. 259 (1995)p. 22
- [19] V. Menchise, G. De Simone, T. Tedeschi, R. Corradini, S. Sforza, R. Marchelli, D. Capasso, M. Saviano and C. Pedone. *Proc. Natl. Acad. Sci.* 100 (12021) p. 2003
- [20] M.M. Green and V. Jain. *Origins Life Evolution Biospheres*. 40 (2010) p. 111. doi: [10.1007/s11084-009-9180-7](https://doi.org/10.1007/s11084-009-9180-7)
- [21] T. Kimura, K. Hamase, Y. Miyoshi, R. Yamamoto, K. Yasuda, M. Mita, H. Rakugi, T. Hayashi and Y. Isaka. *Sci. Rep.* 6 (2016) p. p26137. doi: [10.1038/srep26137](https://doi.org/10.1038/srep26137)
- [22] J.H. Kim and A.R. Scialli. *Toxicol. Sci.* 122 (2011) p. 1. doi: [10.1093/toxsci/kfr088](https://doi.org/10.1093/toxsci/kfr088)
- [23] S.W. Smith. *Toxicol. Sci.* 11 (2009) p. 4. doi: [10.1093/toxsci/kfp097](https://doi.org/10.1093/toxsci/kfp097)

- [24] O.E. Sepelgy, S. Haseloff, S.K. Alamsetti and C. Schneider. *Angew. Chem., Int. Ed.* 53 (2014) p. 7923. doi: [10.1002/anie.201403573](https://doi.org/10.1002/anie.201403573)
- [25] J. Navarro-Sanchez, A.I. Argente-Garcia, Y. Moliner-Martinez, D. Roca-Sanjuan, D. Antypov, P. Campíns-Falcó, M.J. Rosseinsky and C. Marti-Gastaldo. *J. Am. Chem. Soc.* 139 (2017) p. 4294. doi: [10.1021/jacs.7b00280](https://doi.org/10.1021/jacs.7b00280)
- [26] R. Brimiouille, D. Lenhart, M.M. Maturi and T. Bach. *Angew. Chem., Int. Ed.* 54 (2015) p. 3872. doi: [10.1002/anie.201411409](https://doi.org/10.1002/anie.201411409)
- [27] N. Kameta, M. Masuda and T. Shimizu. *Chem. Commun.* 51 (2015) p. 11104. doi: [10.1039/C5CC03843J](https://doi.org/10.1039/C5CC03843J)
- [28] A. Werner. *Eur. J. Inorg. Chem.* 44 (1887) p. 1911
- [29] W. Ma, L. Xu, A.F. De Moura, X. Wu, H. Kuang, C. Xu and N.A. Kotov. *Chem. Rev.* 117 (2017) p. 8041. doi: [10.1021/acs.chemrev.6b00755](https://doi.org/10.1021/acs.chemrev.6b00755)
- [30] G. Cao and Y. Wang, *Nanostructures and Nanomaterials: Synthesis, Properties and Applications*, World Scientific, Singapore, 2004
- [31]. S. Agnihotri, S. Mukherji and S. Mukherji. *RSC Adv.* 4 (2014) p. 3974
- [32] Y. Wang, J. Xu, Y. Wang and H. Chen. *Chem. Soc. Rev.* 42 (2013) p. 2930. doi: [10.1039/C2CS35332F](https://doi.org/10.1039/C2CS35332F)
- [33] D. Bradshaw, J.B. Claridge, E.J. Cussen, T.J. Prior and M.J. Rosseinsky. *Acc. Chem. Res.* 38 (2005) p. 273. doi: [10.1021/ar0401606](https://doi.org/10.1021/ar0401606)
- [34] E.C. Dreaden, A.M. Alkilany, X. Huang, C.J. Murphy and M.A. El-Sayed. *Chem. Soc. Rev.* 41 (2012) p. 2740
- [35] J. Liu, L. Chen, H. Cui, J. Zhang, L. Zhang and C.Y. Su. *Chem. Soc. Rev.* 43 (2014) p. 6011. doi: [10.1039/C4CS00094C](https://doi.org/10.1039/C4CS00094C)
- [36] J.K. Gansel, M. Tiel, M.S. Rill, M. Decker, K. Bade, V. Saile, G. Von Freymann, S. Linden and M. Wegener. *Science.* 325 (2009) p. 1513. doi: [10.1126/science.1177031](https://doi.org/10.1126/science.1177031)
- [37] T.R. Jensen, M.D. Malinsky, C.L. Haynes and R.P. Van Duyne. *J. Phys. Chem. B.* 104 (2000) p. 10549. doi: [10.1021/jp002435e](https://doi.org/10.1021/jp002435e)
- [38] W. Wu, P.N. Njoki, H. Han, H. Zhao, E.A. Schiff, P.S. Lutz, L. Solomon, S. Matthews and M.M. Maye. *J. Phys. Chem. C.* 115 (2011) p. 9933. doi: [10.1021/jp201151m](https://doi.org/10.1021/jp201151m)
- [39] S. Gómez-Graña, C. Fernández-López, L. Polavarapu, J.B. Salmon, J. Leng, I. Pastoriza-Santos and J. Pérez-Juste. *Chem. Mater.* 27 (2015) p. 8310. doi: [10.1021/acs.chemmater.5b03620](https://doi.org/10.1021/acs.chemmater.5b03620)
- [40] Y. Zhao, F. Zhao, X. Wang, C. Xu, Z. Zhang, G. Shi and L. Qu. *Angew. Chem., Int. Ed.* 53 (2014) p. 13934. doi: [10.1002/anie.201409080](https://doi.org/10.1002/anie.201409080)
- [41] O. Gülzeren, F. Ercolessi and E. Tosatti. *Phys. Rev. Lett.* 80 (1998) p. 3775. doi: [10.1103/PhysRevLett.80.3775](https://doi.org/10.1103/PhysRevLett.80.3775)
- [42] Y. Kondo and K. Takayanagi. *Science.* 289 (2000) p. 606. doi: [10.1126/science.289.5479.606](https://doi.org/10.1126/science.289.5479.606)
- [43] E. Tosatti, S. Prestipino, S. Kostlmeier, A. Dal Corso and F.D. Di Tolla. *Science.* 291 (2001) p. 288. doi: [10.1126/science.291.5502.288](https://doi.org/10.1126/science.291.5502.288)
- [44] A.S. Baimuratov, I.D. Rukhlenko, Y.K. Gun'ko, A.V. Baranov and A.V. Fedorov. *Nano Lett.* 15 (2015) p. 1710. doi: [10.1021/nl504066f](https://doi.org/10.1021/nl504066f)
- [45] M. Farrag, M. Tschurl and U. Heiz. *Chem. Mater.* 25 (2013) p. 862. doi: [10.1021/cm3033725](https://doi.org/10.1021/cm3033725)
- [46] D. Bochicchio and R. Ferrando. *Nano Lett.* 10 (2010) p. 4211. doi: [10.1021/nl1017157](https://doi.org/10.1021/nl1017157)
- [47] H. Elgavi, C. Krekeler, R. Berger and D. Avnir. *J. Phys. Chem C.* 116 (2012) p. 330. doi: [10.1021/jp209085r](https://doi.org/10.1021/jp209085r)

- [48] M. Zhang, J. Zhang, T. Gu, H. Zhang, Y. Luo and W. Cao. *J. Phys. Chem. A*. 119 (2015) p. 3458. doi: [10.1021/jp511575y](https://doi.org/10.1021/jp511575y)
- [49] T. Nakashima, Y. Kobayashi and T. Kawai. *J. Am. Chem. Soc.* 131 (2009) p. 10342. doi: [10.1021/ja902800f](https://doi.org/10.1021/ja902800f)
- [50] P.X. Gao, Y. Ding, W. Mai, W.L. Hughes, C. Lao and Z.L. Wang. *Science*. 309 (2005) p. 1700. doi: [10.1126/science.1116168](https://doi.org/10.1126/science.1116168)
- [51] K. Ostrikov and H. Mehdipour. *ACS Nano*. 5 (2011) p. 8372. doi: [10.1021/nn202666w](https://doi.org/10.1021/nn202666w)
- [52] Z. Yu, L. Tetard and L. Zhai. *J. Thomas, Ener. Environ. Sci.* 8 (2015) p. 702. doi: [10.1039/C4EE03229B](https://doi.org/10.1039/C4EE03229B)
- [53] Y. Yang, Y. Zheng, W. Cao, A. Titov, J. Hyvonen, J.R. Manders, J. Xue, P.H. Holloway and L. Qian. *Nat. Photon.* 9 (2015) p. 259. doi: [10.1038/nphoton.2015.36](https://doi.org/10.1038/nphoton.2015.36)
- [54] J.H. Jung, Y. Ono, K. Hanabusa and S. Shinkai. *J. Am. Chem. Soc.* 122 (2000) p. 5008. doi: [10.1021/ja000449s](https://doi.org/10.1021/ja000449s)
- [55] B.J. Ohlsson, M.T. Björk, M.H. Magnusson, K. Deppert, L. Samuelson and L.R. Wallenberg. *Appl. Phys. Lett.* 79 (2001) p. 3335. doi: [10.1063/1.1418446](https://doi.org/10.1063/1.1418446)
- [56] A. Ben-Moshe, B.M. Maoz, A.O. Govorov and G. Markovich. *Chem. Soc. Rev.* 42 (2013) p. 7028. doi: [10.1039/c3cs60139k](https://doi.org/10.1039/c3cs60139k)
- [57] Y. Zheng, L. Lin, X. Ye, F. Guo and X. Wang. *Angew. Chem.* 126 (2014) p. 12120. doi: [10.1002/ange.201407319](https://doi.org/10.1002/ange.201407319)
- [58] C. Gautier and T. Bürgi. *Chem. Phys. Chem.* 10 (2009) p. 483. doi: [10.1002/cphc.200800709](https://doi.org/10.1002/cphc.200800709)
- [59] S. Srivastava, A. Santos, K. Critchley, K. Kim, P. Podsiadlo, K. Sun, J. Lee, C. Xu, G. D. Lilly, S.C. Glotzer and N.A. Kotov. *Science*. 327 (2010) p. 1355. doi: [10.1126/science.1177218](https://doi.org/10.1126/science.1177218)
- [60] A. Kuzyk, R. Schreiber, Z. Fan, G. Pardatscher, E.M. Roller, A. Högele, F.C. Simmel, A.O. Govorov and T. Liedl. *Nature*. 483 (2012) p. 311. doi: [10.1038/nature10843](https://doi.org/10.1038/nature10843)
- [61] K.E. Shopsowitz, H. Qi, W.Y. Hamad and M.J. MacLachlan. *Nature*. 468 (2010) p. 422. doi: [10.1038/nature09540](https://doi.org/10.1038/nature09540)
- [62] S. Liu, L. Han, Y. Duan, S. Asahina, O. Terasaki, Y. Cao, B. Liu, L. Ma, J. Zhang and S. Che. *Nature Commun.* 3 (2012) p. 1215. doi: [10.1038/ncomms2215](https://doi.org/10.1038/ncomms2215)
- [63] B.M. Maoz, R. van der Weegen, Z. Fan, A.O. Govorov, G. Ellestad, N. Berova, E.W. Meijer and G. Markovich. *J. Am. Chem. Soc.* 134 (2012) p. 17807. doi: [10.1021/ja309016k](https://doi.org/10.1021/ja309016k)
- [64] C. Dryzun and D. Avnir. *Chem. Commun.* 48 (2012) p. 5874. doi: [10.1039/c2cc17727g](https://doi.org/10.1039/c2cc17727g)
- [65] A.M. Funston, C. Novo, T.J. Davis and P. Mulvaney. *Nano Lett.* 9 (2009) p. 1651. doi: [10.1021/nl900034v](https://doi.org/10.1021/nl900034v)
- [66] B. Ding, Z. Deng, H. Yan, S. Cabrini, R.N. Zuckermann and J. Bokor. *J. Am. Chem. Soc.* 13 (2010) p. 3248
- [67] A. Querejeta-Fernández, G. Chauve, M. Methot, J. Bouchard and E. Kumacheva. *J. Am. Chem. Soc.* 136 (2014) p. 4788. doi: [10.1021/ja501642p](https://doi.org/10.1021/ja501642p)
- [68] C.L. Chen, P.J. Zhang and N.L. Rosi. *J. Am. Chem. Soc.* 130 (2008) p. 13555. doi: [10.1021/ja805683r](https://doi.org/10.1021/ja805683r)
- [69] T.G. Schaaff, G. Knight, M.N. Shafiqullin, R.F. Borkman and R.L. Whetten. *J. Phys. Chem. B*. 102 (1998) p. 10643. doi: [10.1021/jp9830528](https://doi.org/10.1021/jp9830528)
- [70] Y.N. Li, D.S. Yu, L.M. Dai, A. Urbas and Q.A. Li. *Langmuir*. 27 (2011) p. 98. doi: [10.1021/la104131y](https://doi.org/10.1021/la104131y)
- [71] V. Bonačić-Koutecký, R. Mitrić, C. Bürgel and B. Schäfer-Bung. *Comp. Mat. Sci.* 35 (2006) p. 151. doi: [10.1016/j.commatsci.2004.12.075](https://doi.org/10.1016/j.commatsci.2004.12.075)

- [72] R. Jin. *Nanoscale*. 2 (2010) p. 343. doi: [10.1039/B9NR00160C](https://doi.org/10.1039/B9NR00160C)
- [73] Y. Song, S. Wang, J. Zhang, X. Kang, S. Chen, P. Li, H. Sheng and M. Zhu. *J. Am. Chem. Soc.* 136 (2014) p. 2963. doi: [10.1021/ja413114z](https://doi.org/10.1021/ja413114z)
- [74] L. Jin, D.S. Weinberger, M. Melaimi, C.E. Moore, A.L. Rheingold and G. Bertrand. *Angew. Chem., Int. Ed.* 53 (2014) p. 9059. doi: [10.1002/anie.201404665](https://doi.org/10.1002/anie.201404665)
- [75] R. Jin, C. Zeng, M. Zhou and Y. Chen. *Chem. Rev.* 116 (2016) p. 10346. doi: [10.1021/acs.chemrev.5b00703](https://doi.org/10.1021/acs.chemrev.5b00703)
- [76] W. Kurashige, Y. Niihori, S. Sharma and Y. Negishi. *J. Phys. Chem. Lett.* 5 (2014) p. 4134. doi: [10.1021/jz501941p](https://doi.org/10.1021/jz501941p)
- [77] J.J. Pelayo, R.L. Whetten and I.L. Garzón. *J. Phys. Chem. C.* 119 (2015) p. 28666. doi: [10.1021/acs.jpcc.5b10235](https://doi.org/10.1021/acs.jpcc.5b10235)
- [78] T.G. Schaaff and R.L. Whetten. *J. Phys. Chem. B.* 104 (2000) p. 2630. doi: [10.1021/jp993691y](https://doi.org/10.1021/jp993691y)
- [79] H. Yao. *Curr. Nanosci.* 4 (2008) p. 92
- [80] C. Noguez and I.L. Garzón. *Chem. Soc. Rev.* 38 (2009) p. 757. doi: [10.1039/b800404h](https://doi.org/10.1039/b800404h)
- [81] S. Knoppe and T. Bürgi. *Acc. Chem. Res.* 47 (2014) p. 1318. doi: [10.1021/ar400295d](https://doi.org/10.1021/ar400295d)
- [82] H. Yao. *Prog. Natur. Sci.: Mater. Int.* 26 (2016) p. 428. doi: [10.1016/j.pnsc.2016.08.006](https://doi.org/10.1016/j.pnsc.2016.08.006)
- [83] C.M. Aikens, *Optical Properties and Chirality*, in *Frontiers of Nanoscience Vol. 9: Protected Metal Clusters: From Fundamentals to Applications*, T. Tsukuda and H. Häkkinen, eds., Elsevier, Amsterdam, 2015p. 223
- [84] C. Zeng and R. Jin. *Chem. Asian J.* 12 (2017) p. 1839. doi: [10.1002/asia.201700023](https://doi.org/10.1002/asia.201700023)
- [85] C. Zeng, Z. Wu and R. Jin, *Chirality in Gold Nanoclusters*, in *Chiral Nanomaterials: Preparation, Properties and Applications*, Z. Tang, ed., John Wiley & Sons, Weinheim, 2018p. 99
- [86] S. Knoppe. *Chirality in Ligand-Stabilized Metal Clusters*, *Encyclopedia of Interfacial Chemistry: Surface Science and Electrochemistry, Chapter 12982, Reference Module in Chemistry, Molecular Sciences and Chemical Engineering*. K. Wandelt, ed., Elsevier, Amsterdam, 2018p.406
- [87] S. Riva. *Mater. Sci. Technol.* 33 (2017) p. 795
- [88] I.L. Garzón, J.A. Reyes-Nava, J.I. Rodríguez-Hernández, I. Sigal, M.R. Beltrán and K. Michaelian. *Phys. Rev. B.* 66 (2002) p. 073403. doi: [10.1103/PhysRevB.66.073403](https://doi.org/10.1103/PhysRevB.66.073403)
- [89] M.-R. Goldsmith, C.B. George, G. Zuber and R. Naaman. *Phys. Chem. Chem. Phys.* 8 (2006) p. 63. doi: [10.1039/B511563A](https://doi.org/10.1039/B511563A)
- [90] C. Gautier and T. Bürgi. *J. Am. Chem. Soc.* 128 (2006) p. 11079. doi: [10.1021/ja058717f](https://doi.org/10.1021/ja058717f)
- [91] C.E. Román-Velazquez, C. Noguez and I.L. Garzón. *J. Phys. Chem. B.* 107 (2003) p. 12035. doi: [10.1021/jp0356315](https://doi.org/10.1021/jp0356315)
- [92] P.D. Jadzinsky, G. Calero, C.J. Ackerson, D.A. Bushnell and R.D. Kornberg. *Science*. 318 (2007) p. 430. doi: [10.1126/science.1143609](https://doi.org/10.1126/science.1143609)
- [93] H. Qian, W.T. Eckenhoff, Y. Zhu, T. Pintauer and R. Jin. *J. Am. Chem. Soc.* 132 (2010) p. 8280. doi: [10.1021/ja103592z](https://doi.org/10.1021/ja103592z)
- [94] O. López-Acevedo, H. Tsunoyama, T. Tsukuda, H. Häkkinen and C.M. Aikens. *J. Am. Chem. Soc.* 132 (2010) p. 8210. doi: [10.1021/ja102934q](https://doi.org/10.1021/ja102934q)
- [95] I. Dolamic, S. Knoppe, A. Dass and T. Bürgi. *Nat. Commun.* 3 (2012) p. 798. doi: [10.1038/ncomms1802](https://doi.org/10.1038/ncomms1802)
- [96] A. Sánchez-Castillo, C. Noguez and I.L. Garzón. *J. Am. Chem. Soc.* 132 (2010) p. 1504. doi: [10.1021/ja907365f](https://doi.org/10.1021/ja907365f)

- [97] S. Knoppe, I. Dolamic, A. Dass and T. Bürgi. *Angew. Chem., Int. Ed.* 51 (2012) p. 7589. doi: [10.1002/anie.201202369](https://doi.org/10.1002/anie.201202369)
- [98] C. Zeng, T. Li., A. Das, N.L. Rosi and R. Jin. *J. Am. Chem. Soc.* 153 (2013) p. 10011. doi: [10.1021/ja404058q](https://doi.org/10.1021/ja404058q)
- [99] S. Knoppe, O.A. Wong, S. Malola, H. Häkkinen, T. Bürgi, T. Verbiest and C.J. Ackerson. *J. Am. Chem. Soc.* 136 (2014) p. 4129. doi: [10.1021/ja500809p](https://doi.org/10.1021/ja500809p)
- [100] S. Knoppe, I. Dolamic and T. Bürgi. *J. Am. Chem. Soc.* 132 (2012) p. 13114
- [101] I.L. Garzón, M.R. Beltrán, G. González, I. Gutiérrez-González, K. Michaelian, J.A. Reyes-Nava and J.I. Rodríguez-Hernández. *Eur. Phys. J. D.* 24 (2003) p. 105. doi: [10.1140/epjd/e2003-00187-4](https://doi.org/10.1140/epjd/e2003-00187-4)
- [102] A. Lechtken, D. Schooss, J.R. Stairs, M.N. Blom, F. Furche, N. Morgner, O. Kostko, B. Issendorff and M.M. Kappes. *Angew. Chem., Int. Ed.* 46 (2007) p. 2944. doi: [10.1002/anie.200604760](https://doi.org/10.1002/anie.200604760)
- [103] X. Gu, S. Bulusu, X. Li, X.C. Zeng, J. Li, X.G. Gong and L.-S. Wang. *J. Phys. Chem. C.* 111 (2007) p. 8228. doi: [10.1021/jp071960b](https://doi.org/10.1021/jp071960b)
- [104] I.E. Santizo, F. Hidalgo, L.A. Pérez, C. Noguez and I.L. Garzón. *J. Phys. Chem. C.* 112 (2008) p. 17533. doi: [10.1021/jp806080b](https://doi.org/10.1021/jp806080b)
- [105] A.J. Karttunen, M. Linnolahti, T.A. Pakkanena and P. Pyykkö. *Chem. Commun* (2008) p. 465. doi: [10.1039/B715478J](https://doi.org/10.1039/B715478J)
- [106] X.J. Liu and I.P. Hamilton. *Nanoscale.* 9 (2017) p. 10321. doi: [10.1039/C7NR02868G](https://doi.org/10.1039/C7NR02868G)
- [107] A.B. Buda, T. Auf der Heyde and K. Mislow. *Angew. Chem.Int. Ed. Engl.* 31 (1992) p. 989. doi: [10.1002/anie.199209891](https://doi.org/10.1002/anie.199209891)
- [108] M. Petitjean. *Entropy.* 5 (2003) p. 271. doi: [10.3390/e5030271](https://doi.org/10.3390/e5030271)
- [109] M.H. Jamróz, J.E. Rode, S. Ostrowski, P.F.J. Lipinski and J.C. Dobrowolski. *J. Chem. Inf. Model.* 52 (2012) p. 1462. doi: [10.1021/ci200321u](https://doi.org/10.1021/ci200321u)
- [110] S. Alvarez, P. Alemany and D. Avnir. *Chem. Soc. Rev.* 34 (2005) p. 313. doi: [10.1039/b301406c](https://doi.org/10.1039/b301406c)
- [111] A.B. Buda and K. Mislow. *J. Am. Chem. Soc.* 114 (1992) p. 6006. doi: [10.1021/ja00041a016](https://doi.org/10.1021/ja00041a016)
- [112] I.L. Garzón, K. Michaelian, M.R. Beltrán, A. Posada-Amarillas, P. Ordejon, E. Artacho, D. Sánchez-Portal and J.M. Soler. *Phys. Rev. Lett.* 81 (1998) p. 1600. doi: [10.1103/PhysRevLett.81.1600](https://doi.org/10.1103/PhysRevLett.81.1600)
- [113] I.L. Garzón, C. Rovira, K. Michaelian, M.R. Beltrán, J. Junquera, P. Ordejón, E. Artacho, D. Sánchez-Portal and J.M. Soler. *Phys. Rev. Lett.* 85 (2000) p. 5290. doi: [10.1103/PhysRevLett.85.5250](https://doi.org/10.1103/PhysRevLett.85.5250)
- [114] H. Häkkinen, M. Walter and H. Grönbeck. *J. Phys. Chem. B.* 110 (2006) p. 9927. doi: [10.1021/jp0619787](https://doi.org/10.1021/jp0619787)
- [115] X.K. Wan, S.F. Yuan, Z.W. Lin and Q.M. Wang. *Angew. Chem., Int. Ed.* 53 (2014) p. 2923. doi: [10.1002/anie.201308599](https://doi.org/10.1002/anie.201308599)
- [116] J. Chen, Q.F. Zhang, P.G. Williard and L.S. Wang. *Inorg. Chem.* 53 (2014) p. 3932. doi: [10.1021/ic500562r](https://doi.org/10.1021/ic500562r)
- [117] C. Zeng, Y. Chen, K. Iida, K. Nobusada, K. Kirschbaum, K.J. Lambright and R. Jin. *J. Am. Chem. Soc.* 138 (2016) p. 3950. doi: [10.1021/jacs.5b12747](https://doi.org/10.1021/jacs.5b12747)
- [118] A. Dass, S. Theivendran, P.R. Nimmala, C. Kumara, V.R. Jupally, A. Fortunelli, L. Sementa, G. Barcaro, X. Zuo and B.C. Noll. *J. Am. Chem. Soc.* 137 (2015) p. 4610. doi: [10.1021/ja513152h](https://doi.org/10.1021/ja513152h)
- [119] C. Zeng, Y. Chen, K. Kirschbaum, K. Appavoo, M.Y. Sfeir and R. Jin. *Sci. Adv.* 1 (2015) p. e1500045. doi: [10.1126/sciadv.1500045](https://doi.org/10.1126/sciadv.1500045)
- [120] X. López-Lozano, L.A. Pérez and I.L. Garzón. *Phys. Rev. Lett.* 97 (2006) p. 233401. doi: [10.1103/PhysRevLett.97.233401](https://doi.org/10.1103/PhysRevLett.97.233401)

- [121] L.A. Pérez, X. López-Lozano and I.L. Garzón. Eur. Phys. J. D. 52 (2009) p. 123. doi: [10.1140/epjd/e2008-00289-5](https://doi.org/10.1140/epjd/e2008-00289-5)
- [122] J.J. Pelayo, I. Valencia, G. Díaz, X. López-Lozano and I.L. Garzón. Eur. Phys. J. D. 69 (2015) p. 277. doi: [10.1140/epjd/e2015-60562-0](https://doi.org/10.1140/epjd/e2015-60562-0)
- [123] J. Autschbach and T. Ziegler. J. Chem. Phys. 116 (2002) p. 891. doi: [10.1063/1.1420401](https://doi.org/10.1063/1.1420401)
- [124] J. Autschbach, T. Ziegler, S.J.A. Van Gisbergen and E.J. Baerends. J. Chem. Phys. 116 (2002) p. 6930. doi: [10.1063/1.1436466](https://doi.org/10.1063/1.1436466)
- [125] M.E. Casida, *Time-Dependent Density Functional Response Theory for Molecules*, in *Recent Advances in Density-Functional Methods*, D.P. Chong, ed., World Scientific, Singapore, 1995p. 155
- [126] O. Baseggio, G. Fronzoni and M. Stener. J. Chem. Phys. 143 (2015)p. 024106. doi:[10.1063/1.4923368](https://doi.org/10.1063/1.4923368)
- [127] O. Baseggio, D. Toffoli, G. Fronzoni, M. Stener, L. Sementa and A. Fortunelli. J. Phys. Chem. C. 120 (2016) p. 24335. doi: [10.1021/acs.jpcc.6b07323](https://doi.org/10.1021/acs.jpcc.6b07323)
- [128] A. Rodger and B. Nordén *Circular Dichroism & Linear Dichroism*, Oxford University Press, Oxford, 1997
- [129] A.D. Buckingham. Adv. Chem. Phys. 12 (1967)p. 107
- [130] L. Sementa, G. Barcaro, O. Baseggio, M. De Vetta, A. Dass, E. Aprà, M. Stener and A. Fortunelli. J. Phys. Chem. C. 121 (2017) p. 10832. doi: [10.1021/acs.jpcc.6b12029](https://doi.org/10.1021/acs.jpcc.6b12029)
- [131] S. Theivendran, L. Chang, A. Mukherjee, L. Sementa, M. Stener, A. Fortunelli and A. Dass. J. Phys. Chem. C. 122 (2018) p. 4524. doi: [10.1021/acs.jpcc.8b00556](https://doi.org/10.1021/acs.jpcc.8b00556)
- [132] L. Chang, O. Baseggio, L. Sementa, D. Cheng, G. Fronzoni, D. Toffoli, E. Aprà, M. Stener and A. Fortunelli. J. Chem. Theory Comput. 14 (2018) p. 3703. doi: [10.1021/acs.jctc.8b00250](https://doi.org/10.1021/acs.jctc.8b00250)
- [133] A. Sharma, T. Mori, H.C. Lee, M. Worden, E. Bidwell and T. Hegmann. ACS Nano. 8 (2014) p. 11966. doi: [10.1021/nn504980w](https://doi.org/10.1021/nn504980w)
- [134] N.V. Karimova and C.M. Aikens. J. Phys. Chem. A. 119 (2015) p. 8163. doi: [10.1021/acs.jpca.5b03312](https://doi.org/10.1021/acs.jpca.5b03312)
- [135] X. He, Y. Wang, H. Jiang and L. Zhao. J. Am. Chem. Soc. 138 (2016) p. 5634. doi: [10.1021/jacs.6b01658](https://doi.org/10.1021/jacs.6b01658)
- [136] S. Takano and T. Tsukuda. J. Phys. Chem. Lett. 7 (2016) p. 4509. doi: [10.1021/acs.jpcllett.6b02294](https://doi.org/10.1021/acs.jpcllett.6b02294)
- [137] M.J. Frisch, G.W. Trucks, H.B. Schlegel, G.E. Scuseria, M.A. Robb, J.R. Cheeseman, G. Scalmani, V. Barone, G.A. Petersson, H. Nakatsuji, X. Li, M. Caricato, A. Marenich, J. Bloino, B.G. Janesko, R. Gomperts, B. Mennucci, H.P. Hratchian, J.V. Ortiz, A.F. Izmaylov, J.L. Sonnenberg, D. Williams-Young, F. Ding, F. Lipparini, F. Egidi, J. Goings, B. Peng, A. Petrone, T. Henderson, D. Ranasinghe, V.G. Zakrzewski, J. Gao, N. Rega, G. Zheng, W. Liang, M. Hada, M. Ehara, K. Toyota, R. Fukuda, J. Hasegawa, M. Ishida, T. Nakajima, Y. Honda, O. Kitao, H. Nakai, T. Vreven, K. Throssell, J.A. Montgomery Jr., J.E. Peralta, F. Ogliaro, M. Bearpark, J.J. Heyd, E. Brothers, K.N. Kudin, V.N. Staroverov, T. Keith, R. Kobayashi, J. Normand, K. Raghavachari, A. Rendell, J.C. Burant, S.S. Iyengar, J. Tomasi, M. Cossi, J.M. Millam, M. Klene, C. Adamo, R. Cammi, J.W. Ochterski, R.L. Martin, K. Morokuma, O. Farkas, J.B. Foresman and D.J. Fox *Gaussian 09, Revision A.02*, Gaussian, Inc., Wallingford CT, 2016
- [138] A. Das, C. Liu, H.L. Byun, K. Nobusada, S. Zho, N. Rosi and R. Jin. Angew. Chem., Int. Ed. 54 (2015) p. 3140. doi: [10.1002/anie.201410161](https://doi.org/10.1002/anie.201410161)
- [139] M. Zhu, C.M. Aikens, F.J. Hollander, G.C. Schatz and R. Jin. J. Am. Chem. Soc. 130 (2008) p. 3754

Appendix A. Hausdorff chirality measure

Chirality is a property that depends only on the geometry and is independent of its physical and chemical manifestations. The *Hausdorff chirality measure* (HCM) provides a methodology to quantify chirality, based on the concept of *Hausdorff distance* between sets of points [111].

To obtain a mathematical expression for HCM, we consider the following: Let Q and Q' denote two nonempty and bounded sets of points in E^3 , representing, respectively, two enantiomers of a chiral object, and let $d(q, q')$ denote the *Euclidean distance* between two points: $q \in Q$ and $q' \in Q'$. The *Hausdorff distance* between sets Q and Q' is the smallest number δ that has the following properties: a spherical ball of radius δ centred at any point of Q (Q'), contains at least one point of Q' (Q), and is defined as follows:

$$h(Q, Q') = h(Q', Q) = \max\{\rho(Q, Q'), \rho(Q', Q)\}$$

where

$$\rho(Q, Q') = \sup_{q \in Q} \left\{ \inf_{q' \in Q'} \{d(q, q')\} \right\}, \quad \rho(Q', Q) = \sup_{q' \in Q'} \left\{ \inf_{q \in Q} \{d(q', q)\} \right\}.$$

Obviously $h(Q, Q') = 0$ only if $Q = Q'$, particularly it is zero between objects that are identical, i.e. achiral. By rotating and translating one enantiomorph with respect to the other, one can find the minimal value $h_{\min}(Q, Q')$. If $d(Q)$ is the diameter of Q , i.e. the largest distance between any two points of Q , the HCM is defined as follows:

$$H(Q) = h_{\min}(Q, Q')/d(Q).$$

The numerical implementation of the HCM relies on a set of n points in E^3 , $Q = \{q_i\}$, $i = 1, \dots, n$, with the position of each point q_i defined by its Cartesian coordinates (x_i, y_i, z_i) . The enantiomorph Q' is generated with the inversion operator, and keeping Q fixed, is varied systematically via the translational u, v, w and rotational φ, θ, ω parameters. The determination of $H(Q)$ thus becomes a typical problem of searching for a global minimum on a multidimensional hypersurface:

$$H(Q) = \frac{\min_{u, v, w, \varphi, \theta, \omega} \{h(Q, Q', u, v, w, \varphi, \theta, \omega)\}}{d(Q)}.$$

A suitable way to obtain this global minimum is the Broyden–Fletcher–Goldfarb–Shanno approach, which is an iterative method for solving unconstrained nonlinear optimization problems based on Newton's method.

Further details and examples on calculations of HCM for bare and ligand-protected metal clusters can be seen in Refs. [77,88,101].